

Seasonal dynamics in the Azores-Gibraltar Strait region: a climatologically-based study

L.I. Carracedo^{a,*}, M. Gilcoto^a, H. Mercier^b, F.F. Pérez^a

^a Marine Research Institute (IIM-CSIC), Eduardo Cabello 6, 36208 Vigo, Spain

^b CNRS, Laboratoire de Physique des Océans, Institut Français de Recherche pour l'Exploitation de la Mer (IFREMER), Centre de Brest, C.S. 1007029280 Plouzané, France

*: Corresponding author : L.I. Carracedo, email address : lcarracedo@iim.csic.es
migil@iim.csic.es ; Herle.Mercier@ifremer.fr ; fiz.perez@iim.csic.es

Abstract:

Annual and seasonal mean circulations in the Azores-Gibraltar Strait Region (North-Eastern Atlantic) are described based on climatological data. An inverse box model is applied to obtain absolute water mass transports consistent with the conservation of volume, salt and heat and the equations of the thermal wind. The large-scale gyre circulation (Azores Current, Azores Counter Current, Canary Current and Portugal Current) is well-represented in climatological data. The Azores Current annual mean transport was estimated to be 6.5 ± 0.8 Sv ($1 \text{ Sv} = 10^6 \text{ m}^3/\text{s}$) eastward, exhibiting a seasonal signal with minimum transport in the spring (5.3 ± 0.8 Sv) and maximum transport in autumn (7.3 ± 0.8 Sv). The Azores Current transport is twice that of the Azores Counter Current in spring and autumn and is four-times higher in summer and winter. The southward Portugal and Canary Currents show similar seasonal cycles with maximum transports in spring (3.5 ± 0.6 and 6.6 ± 0.4 Sv, respectively).

The overturning circulation within the area has an annual mean magnitude of 2.2 ± 0.1 Sv and two seasonal extremes; the highest in summer (2.6 ± 0.1 Sv) and the lowest in winter (1.7 ± 0.1 Sv). Of the annual mean, about two thirds (1.4 Sv) of the overturning circulation results from water mass transformation west of the Strait of Gibraltar: the downwelling and recirculation of upper Central Water (0.6 Sv) in the intermediate layer, the entrainment of Central Water (0.6 Sv) into the Mediterranean Outflow and the contribution of Antarctic Intermediate Water (0.2 Sv) to the Mediterranean Outflow. The remaining 0.8 Sv relates to the overturning in the Mediterranean Sea through the two-layer exchange at the Gibraltar Strait. Accordingly, the density level dividing the upper-inflowing and lower-outflowing limbs of the overturning circulation was found to be $\sigma_1 = 31.65 \text{ kg m}^{-3}$ (σ_1 , potential density referred to 1000 db), which is above the isopycnal that typically separates Central and Mediterranean Water ($\sigma_1 = 31.8 \text{ kg m}^{-3}$). In terms of water masses, we describe quantitatively the water mass composition of the main currents. Focusing on the spread of Mediterranean Water, we found that when the northward Mediterranean Water branch weakens in spring and autumn, the westward Mediterranean Water vein strengthens, and vice versa. The maximum net transports of Mediterranean Water across the northern and western sections of the box were estimated at -1.9 ± 0.6 Sv (summer) and -0.8 ± 0.2 Sv (spring), respectively. Within the error bar (0.2 Sv), we found no significant net volume transport of Mediterranean Water across the southern section.

Highlights

► We describe full circulation patterns in the Azores-Gibraltar Strait Region (North-Eastern Atlantic) by means of climatological data. ► We use an inverse box model for obtaining absolute transports consistent with volume, salt, heat conservation and thermal wind equations. ► We solve the main source water masses fractions by means of an extended Optimum Multiparameter Analysis. ► Circulation seasonality is described and main currents quantified. ► We estimate indirectly the entrainment of central waters that leads to an overturning circulation into the enclosed box.

Keywords : Azores Current ; Gibraltar Strait ; Inverse model ; Water masses ; Overturn circulation ; Entrainment

1. Introduction

Progress has been made in understanding ocean dynamics through continuously evolving techniques and methods. Inverse methods were first applied to oceanographic data (in situ temperature and salinity, namely the density field) in the mid-1970s, when it began to be fully recognized that the thermal-wind and conservation equations permitted the estimation of the absolute velocity field as the sum of both the reference level velocity and thermal-wind velocity (Wunsch, 1977, 1978). The inverse box model concept has since been developed, based on both linear and nonlinear procedures (Mercier, 1986; Lux et al., 2001), to provide the best available picture of the global circulation (Ganachaud and Wunsch, 2000). During the 1990s, inverse methods were introduced in the Northeastern Atlantic region to solve the absolute circulation pattern (Arhan et al., 1994; Paillet and Mercier, 1997) and they have since been used widely (Álvarez, 2002; Álvarez et al., 2005, 2009; Hernández-Guerra et al., 2005; Machín et al., 2006a; Lherminier et al., 2007, 2010). In this paper, we focus on the Azores-Gibraltar region; specifically, on a box defined by the World Ocean Atlas 2009 (WOA09) nodes depicted in Figure 1.

The large-scale surface circulation (0 to ~500 m) in the North-Eastern Atlantic region is dominated by an eastward-zonal basin-scale current, the Azores Current (AC), centred at about 34–35°N (Péliz et al., 2005). After crossing the Mid-Atlantic Ridge between 34 and 36°N (Jia, 2000; Smith and Maltrud, 1999) the AC displays high variability as a result of its meandering (Pingree et al., 1999; Alves et al., 2002; Carracedo et al., 2012). The surface circulation in the Gulf of Cadiz (Figure 1) has been interpreted as its last meander (Criado-Aldeanueva et al., 2006). Branches of the AC loop gently into the Portugal Current (PC) and further south into the Canary Current (CC) (Barton, 2001). The PC flows equatorwards, at least in the upper layer, and when it reaches Cape St. Vincent, most of the flow turns east (Criado-Aldeanueva et al.,

2006) but a small part continues southwards in the surface anti-cyclonic circulation cell to join the CC. The eastward flow forms a surface jet along the Gulf of Cadiz slope/shelf break (Gulf of Cadiz Current) (Péliz et al., 2009), providing 40% of the Atlantic water entering the Mediterranean via the shallow surface layer (Barton, 2001; Criado-Aldeanueva et al., 2006; Péliz et al., 2009). The other 60% is provided by an offshore Atlantic vein (Péliz et al., 2009), probably fed by the AC.

At intermediate depths (~500 to ~2000 m), in particular at the Mediterranean Water (MW) level (1100–1200 dbar), there is a poleward flow in the Iberian ocean margin (Ambar and Howe, 1979a, b; Maze et al., 1997; van Aken, 2000b). In this study, we will refer to MW (Ríos et al., 1992; Ambar et al., 1999; Álvarez, 2002; Álvarez et al., 2005; Alves et al., 2011) as the water mass formed in the Gulf of Cadiz (Figure 1) when the pure Mediterranean outflow water (MOW; Zenk, 1975; Rhein and Hinrichsen, 1993; Baringer and Price, 1997; Huertas et al., 2012) spills over the Gibraltar Sill towards the Gulf of Cadiz, entraining considerable amounts of the overlying central water. By the time this recently ventilated intermediate water mass reaches Cape St. Vincent (Figure 1) it is neutrally buoyant (at ~1000 dbar) and from there, it spreads through the entire North Atlantic (Arhan et al., 1994; Fusco et al., 2008). The MW flows mainly northwards along the European western margin, parallel to the bathymetry contours to the Porcupine Bank (53°N); however, it also follows a secondary route associated with the westward/south-westward movement of intermediate anticyclonic eddies (“meddies”) (Shapiro and Meschanov, 1996; Bower et al., 1995, 1997; van Aken, 2000b). Meddies are formed mainly in the vicinity of Cape St. Vincent (Figure 1), induced by the sharp bend of the bathymetry and the presence of canyons (Richardson et al., 2000). From here, most of them tend to spread across the southern domain of the region (Arhan et al., 1995; Richardson et al., 2000). At 20°W, authors such as Tsuchiya et al. (1992) observed that the MW core crosses the meridian at

approximately 37°N at a depth of about 1000 m; however, this has been related to the Azores Counter Current (ACC) rather than to the westward displacements of meddies. At the same depth level, the fresher Antarctic Intermediate Water flows northwards along the African ocean margin, reaching latitudes as far as 34°N (Machín and Pelegrí, 2009). Here we will refer to AA as the diluted core of the Antarctic Intermediate Water, according to Álvarez et al. (2005). Below the MW level and south of 48°N, an anti-cyclonic flow of Labrador Sea Water (LSW) brings this water mass, originally transported by the North Atlantic Current, southwards and then westwards past the Azores Islands (Saunders, 1982; Reid, 1994; Paillet and Mercier, 1997). Remnants of the Iceland-Scotland Overflow Water (ISOW) also enter the eastern North Atlantic from a northern source (van Aken, 2000a).

At deeper levels (>2500 m), the Lower North East Atlantic Deep Water (NEADW_L) circulates under strong constraint by the topography, forming a cyclonic gyre in the northern part of the eastern basin (Dickson et al., 1985; Arhan et al., 1994; Paillet and Mercier, 1997), between the Discovery Gap and the Azores-Biscay Rise (Figure 1). The northward-flowing deep water enters a cul-de-sac, due to the topographic morphology, which leads to deep upwelling along the European and Northwest African continental margin (Arhan et al., 1994; van Aken, 2000a).

In this context, the Strait of Gibraltar plays an important role as a topographic feature that effectively separates the eastern boundary ventilation system of the Atlantic Ocean into the northern and southern regions (Barton, 2001), enabling the connection between the MOW and the AC. The overflow is known to have a dynamical impact on the upper-layer circulation in the subtropical eastern North Atlantic (Jia, 2000), generating an area of convergence and downwelling in the Gulf of Cadiz. In a global thermohaline context, the MW contribution to the Atlantic Ocean is significant. Through mixing, the MW raises salinity of the North Atlantic Ocean intermediate

118 domain, which ultimately transfers some thermohaline signature to the lower
119 Meridional Overturning Circulation limb by means of the North Atlantic Deep Water
120 formation (Reid, 1994). Off the Strait of Gibraltar, the Gulf of Cadiz is the transitional
121 sub-basin where the pure MOW experiences strong mixing with the Eastern North
122 Atlantic Central Water. The Gulf is broadly considered the geographic origin of the
123 MW observed in the North Atlantic (van Aken, 2000b; Fusco et al., 2008). This
124 entrainment of Eastern North Atlantic Central Water leads to an overturning circulation
125 in the region.

126

127 In this study, we seek a better understanding of the coupling between the
128 horizontal circulation in the region between the Azores Islands and the Gibraltar Strait
129 and the overturning circulation within a climatological framework. We make use of the
130 World Ocean Atlas 2009 (WOA09) data to present a description of the seasonal
131 circulation pattern. To reach this objective, the circulation is derived from a two-
132 dimensional inverse ocean model, which solves the velocity at the reference level
133 problem. Unlike previously published studies in this area, the model exploits
134 climatological and seasonal forcing. The application of a geostrophic inverse model to
135 climatological and seasonal data brings some benefits over the use of synoptic data,
136 because it avoids mesoscale-related uncertainties and problems of synopticity. Thus,
137 this novel approach is a powerful tool with which to attain greater insight into the
138 circulation of the region and to check the consistency of the WOA09 dataset with
139 geostrophic dynamics, as well as to examine the results of using water mass mixing
140 analysis as an additional constraint on the inverse model.

141 In the following sections we first present the data and the methods for estimating
142 the transports through the box and for solving the water mass mixing (section 2). Then,
143 we examine and discuss the mean and seasonal circulation patterns in the Azores to
144 Gibraltar Strait region (section 3). Finally, in section 4 we present concluding remarks.

145

146 **2. Data and methodology**147 *2.1. Hydrographic data*

148 Data of in situ temperature, salinity, dissolved oxygen, phosphate, silicate and nitrate
149 come from the WOA09 database (Boyer et al., 2009)
150 (<http://www.nodc.noaa.gov/OC5/WOA09/>). The data on which this atlas is based come
151 from the World Ocean Database 2009 (<http://www.nodc.noaa.gov/OC5/WOD/>).
152 WOA09 is a set of objectively analysed (1° -grid resolution) annual, seasonal and
153 monthly climatological fields at 33 standard depth levels for the world's oceans.
154 Temperature and salinity climatologies are the average of five “decadal” climatologies
155 for the following time periods: 1955–1964, 1965–1974, 1975–1984, 1985–1994 and
156 1995–2006, while oxygen and nutrient climatologies use all available data regardless of
157 the year of observation (“all-data” climatology). The data underwent thorough quality
158 control (Antonov et al., 2010; Locarnini et al., 2010). Values for oxygen and nutrients
159 (NO_3 , PO_4 and SiO_4), reported in ml l^{-1} and $\mu\text{mol l}^{-1}$, respectively, were converted to
160 $\mu\text{mol kg}^{-1}$. From the WOA09 database, a cruise track-like was constructed by selecting
161 adjacent WOA09 grid nodes that formed a box west of the Gibraltar Strait (referred to
162 as the WOA-Box hereafter) (Figure 1). In total, 31 WOA09 nodes were selected as
163 hydrographic “stations” (vertical profiles) for later geostrophic, tracer conservation and
164 water mass mixing computation. Hereinafter, the term “node pair” refers to the mid-
165 point between nodes. In addition, when seasonal or monthly heat storage variations
166 were needed as a term for the inverse model heat constraint, all WOA09 nodes within
167 the box were selected for the computation. For further comparison, the WOA-Box
168 boundaries are approximately coincident with the CAIBOX cruise (Carracedo et al.,
169 2012; Fajar et al., 2012). Not all WOA09 variables are available at all depths for all
170 seasons and months. Below 500 m, no seasonal variability is given for nutrient
171 concentrations and it is the same below 1500 m for temperature, salinity and oxygen.

Therefore, seasonal and monthly nutrients data were complemented between 500–5500 m (levels 15th to 33th) with the corresponding annual node profiles and temperature, salinity and oxygen monthly node profiles were complemented between 1500–5500 m (levels 25th to 33th) with their corresponding seasonal ones.

Other sources of data used in this work were MEDATLAS2002 (<http://www.ifremer.fr/medar/>), for estimating advective salt fluxes at the Gibraltar Strait and the European Centre for Medium-range Weather Forecast 40-Year Reanalysis (<http://www.ecmwf.int/>), the Objectively Analyzed air-sea Fluxes for the Global Ocean (<http://oafux.whoi.edu/>) and the National Center for Environmental Prediction and Atmospheric Research Global Reanalysis data (<http://www.esrl.noaa.gov/>) for air-sea volume fluxes. In addition, the mean Ekman-layer transport induced by the wind drag at the sea surface was calculated from the European Centre for Medium-range Weather Forecast 40-Year Reanalysis database ($2.5^{\circ} \times 2.5^{\circ}$) (Figure 1), which was added to the geostrophic transports after having distributed it equally over the first 30-m depth.

Annual, seasonal and monthly means were computed from wind data (Sep 1957 to Aug 2002).

2.2. The inverse box model

The underlying method behind the inverse model consists of the computation of absolute transports across the WOA-Box boundaries by applying the thermal wind balance to consecutive WOA09 node profiles along the box section and estimating the reference level velocities by use of property conservation equations as constraints (Mercier, 1986; Lux et al., 2001; Lherminier et al., 2007, 2010). Formally, one *a priori* solution -initial guess- for the reference velocities and vertical diffusivities is defined and combined with the constraints (conservation equations) in a generalised nonlinear least squares inverse model through a cost function (J). By the term “conservation equation” we mean a balance between advection and vertical diffusion. The *a priori* solution and the set of constraints are weighted by their associated uncertainty. Finally,

199 the cost function is minimised to estimate the total velocity field across the WOA-Box
200 and we compute the associated uncertainty (the standard error) of the solution.

201 2.2.1. The unknowns

202 The unknowns of the inverse model are:

203 1. The reference level velocity (u_r) normal to the hydrographic lines, for all station pairs
204 (30 pairs).

205 2. The vertical diffusivities K_v at the interface between layers. The layer limits were
206 selected by σ_3 levels, following Álvarez et al. (2005) and Slater (2003) (hereafter, we
207 will use the notation $\sigma_n = \text{value}$ for a potential density of $(1000 + \text{value}) \text{ kg m}^{-3}$ referred
208 to $n \times 1000 \text{ db}$): 1) from 41.430 (~2500 m) to 41.455 (~2800 m), 2) from 41.455 to
209 41.475 (~3000 m), 3) from 41.475 to 41.490 (~3200 m), 4) from 41.490 to 41.505
210 (~2700 m) and 5) from 41.505 to the bottom. A total of five unknown diffusivities are
211 added to the system, which are necessary to compute the diffusive fluxes in the tracer
212 constraints that are written as a balance between the 3D-advection and vertical
213 diffusion.

214 2.2.2. The reference levels

215 The reference level for the thermal wind equations is established *a priori*. Usually, one
216 assumes prior zero velocity at the reference level, provided we select an interface
217 between the water masses moving in opposite directions or it belongs to a water mass
218 with a very low motion. Before inversion, however, the reference level velocities do not
219 have to be compatible with the conservation constraints. After inversion, the velocities
220 at the reference level are no longer zero and they are compatible with the various
221 conservation constraints. The initial selection was set at 3200 dbar ($\sim\sigma_3 = 41.49 \text{ kg m}^{-3}$,
222 $\sim\sigma_4 = 45.84 \text{ kg m}^{-3}$) based on previous studies (Saunders, 1982; McCartney, 1992;
223 Arhan et al., 1994; Álvarez, 2002; Álvarez et al., 2005, 2009; Lherminier et al., 2007,
224 2010). From this first guess, we modified the initial reference level under the criterion
225 that the velocity field obtained from just the thermal wind equations must satisfy the

circulation patterns in the area. The final selection (Figure 2 right panel) combined the broadly used $\sigma_3 = 41.49 \text{ kg m}^{-3}$ ($\sim 3200 \text{ dbar}$) level (node pairs 5 to 17) with a shallower one at $\gamma^n = 27.922 \text{ kg m}^{-3}$ (neutral density level, $\sim 1600 \text{ dbar}$) in the Canary Basin area (node pairs 18 to 29). The latter is the interface level between intermediate and deep waters (Machín et al., 2006a). For the shallower stations off the Portuguese coast (node pairs 1 to 4), the selected level was 1800 dbar (as the lower limit for MW influence). Off the African coast, in the vicinity of the Lanzarote Channel (Figure 1, node pairs 29 to 30), $\gamma^n = 27.3 \text{ kg m}^{-3}$ ($\sim 700 \text{ dbar}$) was used, because it is the interface level between central and intermediate waters (Machín et al., 2006a; Fraile-Nuez et al., 2010).

2.2.3. The constraints

The model was forced to conserve volume and salt in the entire water column. Following Álvarez et al. (2005) and Slater (2003), volume, salt and heat were also constrained to remain conserved within individual density layers (σ_3 , in kg m^{-3}). In general, the uncertainties for these constraints are selected to be as realistic as possible, taking into consideration the smoothed character of the hydrographic data set. Furthermore, independent volume fluxes were included as additional constraints (on the northern section and in near-coast areas). Following Lherminier et al. (2010), a transport of $-0.8 \pm 0.8 \text{ Sv}$ was imposed on the northern section (nodes 1-11) from $\sigma_4 = 45.85 \text{ kg m}^{-3}$ to the bottom. This transport agrees with McCartney et al.'s (1991) estimation of 0.83 Sv for $\theta < 2.5^\circ\text{C}$ at 36°N between 16 and 19°W . For the eastern boundary of the northern section (nodes 1-3) $-1 \pm 1 \text{ Sv}$ from $\sigma_2 = 36.94 \text{ kg m}^{-3}$ to the bottom was set following Lherminier et al. (2010). On the southern section, seasonally varying climatological values from direct estimates for the Eastern North Atlantic Central Water and AA in the Lanzarote passage area (Fraile-Nuez et al., 2010) were included. Finally, the deep water mass conservation was reinforced by adding a new constraint, which involved an extended Optimum Multiparameter (eOMP) solution. The eOMP method (Karstensen and Tomczak, 1998) consists of quantifying the fractions of a

specific set of source water masses that may compose each sampled water parcel. This method accounts for the non-conservative character of some of the parameters (O_2 , NO_3 , and PO_4) by taking into consideration the biogeochemical processes; this is done by means of Redfield ratios. The eOMP used here (for further details see Carracedo et al., 2012; Pardo et al., 2012;) includes a combination of both classical (θ , S, SiO_4 , NO_3 , PO_4) and extended (θ , S, SiO_4 , O_2^o , NO_3^o , PO_4^o - the last three being the preformed values for these variables) OMP. The variables are weighted in function of their associated uncertainty. Also, the resolution algorithm of the method implements an iterative procedure to successively reduce the residuals on the nutrient balances (Pardo et al., 2012). As a constraint to the minimisation process, mass conservation must be rigorously satisfied and the contribution of each source water mass must be positive. The resulting water mass contribution matrix (with values in the range 0–1), gives the amount of a certain water mass implicated in the mixing process. With this new “weighting” matrix, one can constrain a specific water mass transport without assuming that one water mass is purely delimited by density boundaries; thus, providing an additional constraint to the inverse model. Here, the model was constrained to conserve the sum of deep waters: $LSW + ISOW + NEADW_L$. Previously addressed by studies such as that by Álvarez et al. (2005), this methodology leads to a more detailed constraint on deep water transports, providing favourable feedback to the inverse model. To be consistent with the volume errors by layers, an uncertainty of ± 0.2 Sv was finally established.

2.2.4. Final model set-up

Two approaches were undertaken in this study. The first, labelled as Test 0 (T_0), focussed on reproducing the model configuration used by Slater (2003) (hereinafter referred to as S03), who used Levitus climatology data in a similar box. This approach departs from the “simplest” reference level configuration. Only constraints of volume, heat and salt conservation in deep layers ($> \sim 2500$ m), plus surface-to-bottom volume

280 and salt conservation, were included. On this basis, the choice of uncertainty amplitude
281 let us force a solution equivalent to that of S03 where the volume was constrained to
282 zero, which resulted in a net salt flux across the boundaries of the WOA-Box.
283 Therefore, in T_0 , the zero net volume transport uncertainty was assigned a value of ± 0.1
284 Sv. The salt constraint was defined as the net salt transport obtained by S03's
285 annual/seasonal solutions with a 10% uncertainty (Ganachaud et al., 2000, without their
286 factor of 4). As such, a small volume conservation uncertainty could push the limits of
287 what is physically consistent; therefore, we have decided to keep this solution just for
288 the discussion.

289 The second approach, our best solution, called Test 1 (T_1), changes the way in which the
290 surface-to-bottom volume and salt conservation assumptions are settled. It is more
291 consistent physically in that the excess of evaporation (E) over precipitation (P) and
292 runoff (R) in the region of the WOA-Box and Mediterranean Sea is compensated by a
293 net water transport into the box and not through a net salt flux. In terms of the model,
294 this is applied by strictly conserving salt ($0 \pm 10^6 \text{ kg.s}^{-1}$) and by requiring the volume to
295 account for the E-P-R term with an uncertainty of ± 1 Sv. Moreover, this configuration
296 uses a different *a priori* reference level, chosen after a sensitivity test was applied,
297 which includes the additional independent volume constraints taken from the
298 bibliography. Table 1 summarises these two configurations.

299 *The a priori solution*

300 Ultimately, lateral continuity of the velocity at the reference level after inversion
301 depends on the uncertainty we assume *a priori* for each reference level. For both tests,
302 the *a priori* error for the reference level velocities was selected to be 0.3 cm/s. As S03's
303 solution did not include uncertainties in the computations, 0.3 cm/s is a value that
304 comprises the highest velocity at the reference level obtained with their solution. This
305 value is also consistent with the weak circulation implied by the use of climatology
306 (Figure 2). In the case of T_1 , the velocity errors *a priori* in coastal pairs were doubled to

0.6 cm/s to account for higher uncertainty in these areas. The velocities at the reference level and their errors after inversion (for T_0 and T_I) are shown in Figure 2.

The vertical diffusivity term K_v was set *a priori* to a generalised value of $10^{-4} \pm 10^{-4} \text{ m}^2 \text{ s}^{-1}$ for all the interfaces between the layers (Mazé et al., 1997; Polzin et al., 1997; Lux et al., 2001) and for both tests. After inversion, we obtained higher values (ranging between $1.5 - 2.0 \times 10^4 \text{ m}^2 \text{ s}^{-1}$) than the *a priori* ones as could be expected for a box including strong interactions between currents and topography (Polzin et al., 1997).

In summary, a total of 35 unknowns, velocities at the reference level for 30 nodes pairs, 5 diffusion coefficients for the interfaces between the 6 defined layers and 17 (T_0) or 22 (T_I) constraints comprise the system (Table 1). Therefore, the cost function (J) could be expressed as:

$$J = \sum_{ip=1}^{N_{pair}} \left(\frac{u_r^{ip} - u_{r_0}^{ip}}{\sigma_{u_{r_0}^{ip}}} \right)^2 + \sum_{ii=1}^{N_{interface}} \left(\frac{K_v^{ii} - K_{v_0}^{ii}}{\sigma_{K_{v_0}^{ii}}} \right)^2 + \left(\frac{T^{sb} - T_0^{sb}}{\sigma_{T_0^{sb}}} \right)^2 + \sum_{ip=1}^{N_{pair}} \int_{z_i}^{z_{ii}} \left(\frac{T^{layer} - T_0^{layer}}{\sigma_{T_0^{layer}}} \right)^2 + \sum_{iocom=1}^{N_{other_constraints}} \sum_{ip=L}^M \int_{z_{int}}^{z_{sup}} \left(\frac{T^{ocon} - T_0^{ocon}}{\sigma_{T_0^{ocon}}} \right)^2$$

Subscript 0 means *a priori* established values and σ indicates the uncertainty on these *a priori* values, u_r^{ip} is the reference level velocity at node pair ip after inversion, K_v^{ii} is the vertical diffusion coefficient at interface ii after inversion, T^{sb} represents the surface-to-bottom (*sb*) volume, salt and heat conservation constraints after inversion, T^{layer} are the conservation constraints (volume, salt and heat) by layers and are the specific transports included as additional constraints (other constraints, *ocon*, where deep water masses conservation is also included). The transports shown hereinafter will be taken as positive entering the box.

3. Results and discussion

One important consideration when we work with climatological data is the smoothed character of the thermohaline gradients. This impacts the results directly in terms of weaker geostrophic velocities and a greater reduction of mesoscale variability than would be found in a synoptic cruise; however, the impact is partially compensated,

in terms of volume transport, by the widening of the currents. Of particular concern with these data is the transport of salt, especially in this area of the ocean. The dispersion of MW in the Atlantic Ocean is known to be reinforced by the action of mesoscale meddies detaching from the Mediterranean Undercurrent (Ambar et al., 1999). Lateral intrusive mixing at the eddy boundaries and to a lesser extent, double-diffusive mixing, are responsible for most of their salt and heat loss (Armi et al., 1989). It is worth noting that most of the data used to derive the WOA09 dataset were acquired after the 1970's, when quality control algorithms were adapted to cope with the existence of the meddies; therefore, they are expected to have been properly included in the climatology (in averaged form). The reduction of the mesoscale signal in the climatological data set means that the horizontal salt fluxes at mid-depths are underestimated, which means that the present results may be considered as lower bound estimations.

In the following, we show the main results for our best model configuration (T_I) in terms of the main surface/subsurface currents; the error bars account for the differences with the T_0 solution. Only the significant differences between the two models will be highlighted in the text. Furthermore, note that subsection 3.1.1 will be presented as a validation section as well, providing robustness to the results.

3.1. Velocity field and volume transports

3.1.1. Surface –subsurface horizontal circulation

The absolute velocity fields that results from the annual and seasonal inversions (test T_I) are shown in Figure 2. At intermediate and upper levels (surface to ~2000 m), the main currents represented by the climatological data are AC, ACC, PC and CC (see labels over top contour at Figure 2). The lower latitudes of the western section are occupied by the inflowing AC. Below the AC (approximately at 1000 m) and further north, there is a westward current that can be directly associated to the ACC (Onken, 1992). On the northern section, the southward-flowing PC and the predominantly winter and autumn

360 Iberian Poleward Current (Haynes and Barton, 1990) may be identified. Finally,
361 flowing out of the WOA-Box across the southern section, the CC may be identified.

362 *3.1.1.1. Azores Current*

363 The AC appears, between 1500 and 2000 km from node 1, to be confined mostly to the
364 upper 1000–1500 dbar. For computing the AC transport, we prepared a grid with a
365 resolution of 1 dbar \times 0.01° (latitude degrees). Then, the eastward transports higher than
366 0.001 Sv between 30–37°N, the range in which the AC was identified graphically, were
367 integrated for annual, seasonal and monthly climatologies (see monthly AC variability
368 in Figure 3a). The AC transport is known to range from 9 to 12 Sv between 30–40°W
369 and reduces to around 3–4 Sv closer to the African coast (New et al., 2001). In this
370 work, the annual AC transport was quantified as 6.5 ± 0.8 Sv at 19.5°W, which is close to
371 that obtained by Pingree et al. (1999) from the WOA94 data base (6.7 Sv, with
372 reference level of 2000 dbar) and not far from other estimates derived from
373 hydrographic cruises (9.3 ± 2.6 Sv at 20°W (Carracedo et al., 2012), 6.8–7 Sv at 21–
374 19°W (Alves et al., 2002)). Its broadened width prevents us establishing a precise
375 latitudinal position; however, if we compute a value for the AC core width, that is, the
376 area of velocities higher than 2 cm/s, we find it is narrowest in spring and widest in
377 autumn. In addition, in spring, the AC velocity maximum is the lowest (2.7 cm/s), the
378 current narrows (~240 km) and its maximum depth is minimal (~790 m); therefore, the
379 net AC transport is lower (5.3 ± 0.8 Sv), particularly in June (2.5 ± 0.4 Sv). From this
380 minimum transport in spring, it increases gradually during summer, reaching a
381 maximum in autumn when, regardless of the test, the seasonal AC velocity maximum is
382 higher (~3.2 cm/s) and the current is deeper (~1100 m) and broader (~400 km),
383 resulting in higher transport (7.3 ± 0.8 Sv), which is in agreement with Klein and Siedler
384 (1989). On a monthly basis, we find a relative maximum in September (9.0 ± 0.9 Sv) but
385 an absolute maximum in January (10.2 ± 0.9 Sv) (Figure 3a). Although the AC appears
386 broader than it really is, it exhibits a coherent seasonal variability.

387 Following previous studies (Onken, 1992; Paillet and Mercier, 1997, Alves et al., 2002;
388 Pérez et al., 2003; Kida et al., 2008; Carracedo et al., 2012) and despite the controversy
389 over its permanent existence (Alves et al., 2002), the subsurface westward stream north
390 of the AC, is associated with the ACC (Onken, 1992). An equivalent procedure, such as
391 that used for estimating the AC was followed for the ACC, computed in this case as the
392 integrated outflowing transport in the first 1800 dbar between 36 and 40°N. This
393 current, irrespective of the test (T_0 or T_I), appears intensified in spring (-3.1 ± 0.9 Sv) and
394 autumn (-3.6 ± 0.8 Sv) with lower transport in summer (-1.9 ± 0.7 Sv) and winter ($-$
395 1.7 ± 0.8 Sv). In autumn, the ACC is most intense and easiest to identify as a westward
396 jet. Previous estimations of ACC transport by Alves et al. (2002) were in the range 2–5
397 Sv. They gave a specific transport for a July hydrographic survey of 2.6 Sv at 21°W.

398 Although the monthly variability of the AC and ACC does not seem obviously
399 related (Figure 3a), a ratio (not shown) between both flows was estimated by season. In
400 spring and autumn, the AC transport is twice that of the ACC. On the other hand, during
401 winter and summer, the AC transport is four times higher than that of the ACC. The
402 transport ratio variability is higher in summer (1.4 std), and lower in autumn (0.7 std).
403 The higher variability of the AC/ACC ratio in summer could be understood as the
404 enhanced meandering character of the AC during this season, as identified by Klein and
405 Siedler (1989). Again, comparing with the work of Alves et al. (2002) at 21°W, their
406 computed AC/ACC transports led to a ratio of 2.6 (July). Comas-Rodríguez et al.
407 (2011) gave an AC transport in October 2009 of 13.9 Sv and an ACC of 5.5 Sv
408 (24.5°W), resulting in an AC/ACC ratio of 2.5. The significance of this ratio on the
409 seasonal scale needs further investigation. Based on the present study, we suggest that
410 the AC transports twice as much as the ACC in spring (slightly more) and autumn
411 (slightly less), while ratios of higher-than-two in these surface circulations occur in
412 summer and winter.

413 3.1.1.2. *Portugal Current*

414 The PC transport was estimated as the integrated inflowing transport in the first 1100
415 dbar through the northern section. This current exhibits seasonal variability with a
416 maximum in spring (3.5 ± 0.6 Sv, seasonal mean), reaching a maximum transport of
417 5.20 ± 0.3 Sv in April (monthly mean, Figure 3b). This maximum may be related to the
418 upwelling regime that reinforces the southward coastal branch of this current (Barton,
419 1998, 2001; Navarro-Pérez and Barton, 2001). From spring to autumn/winter, the PC
420 transport weakens to reach minimum values of $0.81 \pm 0.2/0.99 \pm 0.3$ Sv. Stramma and
421 Siedler (1988) estimated a mean autumn value (west of 35°W for the upper 200 m) of
422 1.4 Sv and a mean annual value (between 20°W and the coast) of 2 Sv. This annual
423 mean is slightly higher but comparable with the annual mean computed in this case
424 (1.5 ± 0.4 Sv).

425 The presence of a winter Iberian Poleward Current at the central water level off
426 the Iberian coast has been reported widely (Haynes and Barton, 1990; Mazé et al., 1997;
427 Barton, 1998, 2001; van Aken 2000b; Pérez et al., 2001; Alvarez-Salgado et al., 2003;
428 Péliz et al., 2003). This northward flow forms part of the PC system and it reduces the
429 net PC southward transport in autumn/winter. With our T_I solution, we computed the
430 Iberian Poleward Current transport as the northward flowing waters above 300 m with
431 salinities higher than 35.8, following Pérez et al.'s (2001). For autumn and winter, a
432 transport of 0.2 ± 0.1 Sv with a maximum in January of 1 ± 0.1 Sv were found, while it
433 was absent between the months of May to August. For a similar location, Frouin et al.
434 (1990) estimated a geostrophic transport (referenced at 300 dbar) for this current of 0.5–
435 0.7 Sv.

436 3.1.1.3. *Canary Current*

437 The CC transport was computed as the integrated outflowing transport above 600 dbar
438 on the southern section and the southern part of the western section, south of 32°N . An
439 annual mean transport of -4.0 ± 0.4 Sv was obtained with a minimum in January ($-$
440 3.4 ± 0.4 Sv) and a maximum in June (-8.0 ± 0.4 Sv) (Figure 3b). Using an inverse model,

441 Paillet and Mercier (1997) estimated a mean spring-summer CC transport of about 6 Sv,
442 which is in agreement with our spring-summer estimation (6.0 ± 0.4 Sv).
443 The CC is stronger in summer near the African coast, east of the Canary Islands,
444 whereas in winter, its maximum migrates to the west of the Canaries (Barton, 1998;
445 Navarro-Pérez and Barton, 2001; Machín et al., 2006a). Our results indicate that the
446 lowest CC transport near the shore (15°W to 12°W) of $0.7/1.6$ Sv occurs in
447 autumn/winter, as was also found by Machín et al. (2006a), who estimated a minimum
448 net southward flow for an equivalent width (from surface to ~ 700 m) of $0.9/1.5$ Sv
449 (their Figure 20b,c). They also reported a strong cyclonic eddy recirculation west of
450 Lanzarote and Fuerteventura in spring and an autumn westward migration of the CC
451 branch, as seen in the WOA09 data (see Figure 2 left panel, spring and autumn). This
452 recirculation allows a northward volume flux (surface to 700 m) between the Canary
453 Islands and the African coast estimated (from surface to ~ 700 m) at 0.8 Sv, as compared
454 with 1.8 ± 0.1 Sv (Machín et al., 2006a). As has been seen, both the PC and CC exhibit
455 similar seasonality with a positive significant correlation (95% confidence interval) of
456 66% (Table 2).

457 In general terms, all transports given by our estimations from seasonal
458 climatological inversions agree reasonably well with those seasonal quasi-synoptic
459 cruise-derived transports in the same area. This validates the idea that climatological
460 data can be used to establish a seasonal characterisation (lower-bound estimations) of
461 the principal geostrophic currents.

462 3.1.2. Vertical circulation structure

463 The main vertical structure of the circulation across the limits of the WOA-Box consists
464 of an upper inflowing layer above ~ 500 m (Figure 2 right panel) and an intermediate
465 outflowing layer between ~ 500 and ~ 2000 m. Generally, bottom waters present weak
466 flow (< 0.5 cm/s), except in the Canary Basin (12 – 19.5°W), where an enhanced
467 recirculation of deep waters in summer can be discerned (Figure 2 left panel, summer).

468 The vertically accumulated transports allow us to quantify the overturning circulation in
469 the box (OC, hereinafter). OC can be defined as the magnitude of the upper inflow into
470 the box (Slater, 2003; Álvarez et al., 2005); however, here, we calculate it by
471 accumulating the transport (by pressure and density anomaly levels) from bottom to
472 surface, because the non-zero net transport would be expected to be mainly a
473 consequence of the surface large-scale circulation through the limits of the box.
474 If we compare the OC values obtained by the two integration methods (pressure and
475 density), they differ by 0.4 Sv as a maximum. As the OC is a measure of the conversion
476 of lighter waters into denser waters as they entrain in deeper levels, as well as water
477 masses spread by isopycnal levels, it seems to be more reliable to consider OC transport
478 in terms of density layers. The vertical accumulation of the net transport in the box by
479 density layers (Figure 2 right panel, right chart) allows us to separate the OC in its upper
480 inflowing and lower outflowing limbs by the $\sigma_1 = 31.65 \text{ kg m}^{-3}$ isopycnal layer
481 (hereinafter σ_{OC} will be used to designate the isopycnal of the OC maximum). The
482 annual mean magnitude of the OC into the box is 2.2 ± 0.2 Sv (slightly higher when
483 considering T_0 , 2.5 ± 0.2). In summer, we find the highest OC for both tests (2.6 ± 0.2 and
484 3.3 ± 0.2 Sv); nevertheless, the minimum OC differs between the tests. It occurs in
485 autumn (1.8 ± 0.2 Sv) in the case of T_0 , whereas T_1 , the same OC is found for the other
486 three seasons (1.7 ± 0.2 Sv).

487 3.2. *Water masses circulation*

488 The potential temperature/salinity (θ/S) diagrams in Figure 4 allow us to describe
489 spatially the annual mean hydrography. We depict the transport field (T_0 vs. T_1 velocity
490 field solution) in the θ/S diagrams as coloured contours giving us a first general
491 perspective of the dynamics in the WOA-Box. From north to south, surface waters
492 (above $\sigma_1 = 31.8 \text{ kg m}^{-3}$ isopycnal, central water layer) increase their temperature and
493 salinity whereas the salinity of intermediate waters (between $\sigma_1 = 31.8$ to $\sigma_1 = 32.25 \text{ kg}$
494 m^{-3} , MW layer) diminishes. In the northern section, the highest salinity (36.192) is

found at the MW level. The highest surface thermohaline variability occurs along the western section because of the meridional gradient (frontal zone area). In the climatological annual mean, the Azores Front (Pérez et al., 2003) has been located between 34–35°N (between node pairs 17 and 18), associated with the maximum AC velocity (34°N).

The general circulation pattern that can be deduced is that southern-origin surface waters (those above $\sigma_1 = 31.8 \text{ kg m}^{-3}$), Madeira Mode Water (MMW, Siedler et al., 1987) and Subtropical Eastern North Atlantic Central Water (ENACW_T, Ríos et al., 1992), recirculate clockwise all year round, entering the box through the western section (Figure 4c, 4d) and exiting through the southern section (Figure 4e, 4f). This result is independent of the test and therefore, the upper anticyclonic circulation pattern is well determined. The isopycnal level that separates the upper and lower limbs of the OC ($\sigma_1 = 31.65 \text{ kg m}^{-3}$) is above the isopycnal interface between the central water and MW layers ($\sigma_1 = 31.8 \text{ kg m}^{-3}$). Therefore not all the OC into the WOA-Box can be assigned to water mass transformation. Part of the inflowing central water downwells inside the box, leading to a recirculation of the lower central water bound (between 31.65 and 31.8 kg m^{-3}) out of the box.

At intermediate levels (between the isopycnals of $\sigma_1 = 31.8$ and $\sigma_1 = 32.25 \text{ kg m}^{-3}$), MW leaves the box following two principal paths: one through the northern section (Figure 4a, 4b; northern MW branch, MW_{nb}) and the other through the western section (Figure 4c, 4d; westward MW branch, MW_{wb}). The MW_{wb} recirculates and therefore, more pure MW leaves the box but more mixed/diluted MW re-enters.

Regarding the bottom water circulation, there is a marked pattern with deep water coming through the western section and leaving the region through the northern section (Dickson et al., 1985; Álvarez et al., 2005). Firstly, for T_I , deep waters enter through the western section and leave the box mainly across the northern section. Conversely, both western and southern sections present deep water recirculation in the

case of T_0 . For a quantitative description of these water mass transports we will use the eOMP solution in the next section.

3.2.1. Water masses contribution

The annual mean spatial water mass distribution based on the eOMP run is shown in Figure 5a. MMW is present along the southwestern corner of the WOA-Box, covering the upper 250 dbar of the water column. Following at depth, the ENACW_T reaches its maximum contribution near 250 dbar on the southern section and its range in depth diminishes towards the north, where it is found at the surface. In the range 100–700 dbar, H (Ríos et al., 1992, in honour of Harvey) marks the transition from subtropical (shallower) to subpolar (deeper) central waters. Its higher northward contribution marks the location where the frontal area between both varieties occurs. The main core of the colder subpolar variety of the Eastern North Atlantic Central Water (ENACW_P, Ríos et al., 1992) lies close to 900 dbar, being eroded by the spread of the MW. The AA core is found just below 1000 dbar, in the southern and southwestern parts of the box with a maximum contribution of 45% in the vicinity of the Canary Archipelago. The MW core is located just above 1000 dbar with its highest contribution (up to 73%) on the northern section, i.e., it suffers a 27% dilution from its formation in the Gulf of Cadiz. The main water mass cores are coincident with the western and northern branches of the MW tongue. The westward branch is connected to the ACC, as we will see in following sections. The highest contribution of LSW (80%) is found in the northwestern corner of the box. Another core appears in the southern section, possibly related to some northeastern recirculation of the LSW, as we will discuss later. Finally, NEADW_L occupies the entire deep water column below 2000 dbar with a contribution above 70%. In volumetric terms, the percentage of the water column with respect to the entire section area occupied by each water mass remains quite stable despite the season of the year (seasonal values not shown, annual values in Figure 5a).

3.2.2. Coupling inverse box model - eOMP solution

549 After solving the water mass contributions with the eOMP, we estimate water mass
550 transports by multiplying the percentages field by the absolute volume transports field.
551 In this way, we evaluate whether it is possible to obtain consistent results by combining
552 eOMP with the inverse model solution (in terms of climatological WOA09 data). To do
553 this requires both the interpolation of the vertical standard-level percentages matrix to a
554 depth resolution of 1 dbar and a horizontal averaging of every pair of nodes; thus,
555 matching the volume transport field.

556 In Figure 5b, the seasonal net water mass transports are shown for test T_l . Test T_0
557 net transports are only shown for annual means (see grey bars). MW is always leaving
558 the box with maximum net outflowing transport in summer (-1.6 ± 0.2 Sv) and the
559 minimum in spring (-0.6 ± 0.1 Sv). Central water maximum net inflowing transport also
560 occurs in summer (1.8 ± 1.2 Sv). The total transport of AA across the section is nearly
561 zero. However, the net positive transport found in summer and in the annual mean
562 (0.2 ± 0.2 Sv), could support the hypothesis that the diluted form of AA contributes to
563 MW formation in the region of the Gulf of Cadiz (Louarn and Morin, 2011). Major
564 discrepancies between T_0 and T_l come from the LSW net transport. As we know, LSW
565 cannot be formed inside the WOA-Box; thus, a negative net transport for this water
566 mass could be a sign that the T_0 approach is less appropriate.

567 To evaluate further the seasonal/monthly upper circulation of the WOA-Box, we
568 estimated the relative contribution of each water mass transport to the total transport for
569 each current delimited and described in section 3.1.1 (AC, ACC, PC and CC). The AC
570 transports mainly central water ($\sim 90\%$) with $\sim 50\%$ comprised of the subtropical variety
571 inside the box. The maximum contribution of ENACW_T to AC occurs in spring (57%),
572 whereas the proportion of MMW increases in summer (24%). The MW recirculates into
573 the AC with a maximum 6% of the total AC transport in the autumn-winter period. The
574 ACC exports central water ($\sim 40\%$), in this case mainly the subpolar variety (maximum
575 contribution in autumn, 46%); an important contribution of 25% is MW and LSW

(~20%), which also recirculates out of the box. Both PC and CC currents transport mainly central water (> 95%). During spring, the contribution of $ENACW_P$ to the PC exceeds that of $ENACW_T$, whereas during the autumn-winter period, this proportion reverses. In addition, the PC has little presence of MW (2% the annual mean and up to 8% in spring). On the other hand, ~60% of the CC transport is $ENACW_T$, which recirculates from the AC. The MMW contribution increases in autumn at the expense of the drop in the $ENACW_T$ contribution.

3.2.3. The overturning circulation system in the WOA-Box

As shown in section 3.1.2, the annual mean for the OC into the box was 2.2 ± 0.1 Sv with a maximum OC in summer, 2.6 ± 0.1 Sv, and a minimum in winter, 1.7 ± 0.1 Sv (Figure 6c). This OC variability is in good agreement with that estimated by S03.

Considering the MW as one of the main components of the OC system, acting as main exporter of salt at the intermediate level, we evaluate the role of each of its main branches (Figure 6a, Figure 7). The maximum MW_{nb} net transport takes place in summer (-1.9 ± 0.2 Sv), whereas the MW_{wb} transport is higher in spring (-0.8 ± 0.2 Sv). When the northern branch transport is smaller, the westward branch transport is higher and vice versa. On the annual scale, MW_{nb} and MW_{wb} transports are -0.9 ± 0.3 Sv and -0.4 ± 0.2 Sv, respectively, which are translated into a salt export of 33.1 ± 8 and 15.8 ± 3 Sv psu, respectively. There was no net MW transport across the limits of the southern section (within the errors bars).

The monthly time series of the MW and central water net transports are shown in Figure 6b. A high significance correlation is found between both net transports ($r^2 = 0.90$) with 95% confidence interval (Table 2). The Gibraltar MOW (MOW and the central water inflow at Gibraltar Strait are those given by Soto-Navarro et al., 2010) presents a maximum volume transport in April (García-Lafuente et al., 2007), representing a particular seasonal “pulse” of salty water to MW formation in the Gulf of Cadiz. The higher the net central water incoming flow and the higher the MW outflow

are, the higher the OC is ($r^2 = 0.94$ for correlation for OC/central water pair, $r^2 = 0.88$ for correlation for OC/ MW pair). In addition, the maximum central water entering the box during summer coincides with the maximum central water inflow through the Strait of Gibraltar, i.e., the greater the amount of central water entering the box, the greater the amount of central water entering the Strait of Gibraltar.

Going further in the comprehension of the OC system, two (3D and zonal) schemes show the upper-intermediate circulation (Figures 7 and 8, respectively). Figure 7 complements the results described until now, providing a general perspective of the main flows at two upper (central waters) and lower (MW and AA) horizontal levels. Figure 8 extends the results, summarizing the fluxes that take part of the OC in a simplified zonal diagram. In this figure two areas were delimited: WOA09-Box and a Gibraltar Strait box. From our results, the net Central Water transport ($MMW + ENACW_T + ENACW_P$) across the western limits of the WOA09-Box (northern, western and southern sections) was 1.4 Sv (annual mean). As the transformation of central water in intermediate water takes place within the region of the Gulf of Cadiz (Rhein and Hinrichsen, 1993; Alves et al., 2011), we assume that this net amount of Central Water would be available to reach that region and to take part in the entrainment and/or the Atlantic inflow to the Mediterranean Sea. Therefore, the entrainment (downwelling and mixing) in the Gulf of Cadiz region was approximated as the net inflow of central water into the WOA-Box, minus E-P-R over the WOA-Box superficial area and minus the central water inflow at the Gibraltar Strait. In terms of annual mean, net central water transport in the upper layer (0–500 dbar) was estimated at 2.0 ± 0.2 Sv. From the 2.0 ± 0.2 Sv of the central water net transport, 0.8 ± 0.06 Sv (Soto-Navarro et al., 2010) enters the Mediterranean Sea and thus, the rest (1.2 Sv) is destined to downwell to the intermediate layer. Part of this downwelled water recirculates without mixing with MOW (0.6 ± 0.1 Sv) and the rest (0.6 ± 0.1 Sv) would be mixed with MOW to form MW. Rhein and Hinrichsen (1993) used a local mixing model to describe the mixing of

the MW undercurrent with the overlying NACW, using MOW as one end-member (13.35 °C, 38.40 psu) and a mixture of Atlantic water from different depths above the undercurrent as the other end-member. The percentage of MOW obtained from that model at 7°30'W was 34% (for MW lower core). With this dilution factor, we approximated an “expected” MW outflow (water stabilised in the Gulf of Cadiz at 1100 dbar with properties of 11.74 °C, 36.5 psu). In this approximation, we considered the mean annual MOW transport at the Gibraltar Strait (0.78 ± 0.05 Sv, Soto-Navarro et al., 2010) and took into account that 82% of this overflow comes from “pure 38.40 psu MOW”, which then undergoes mixing and entrainment in the Strait (Huertas et al., 2012). The volume of MW likely to flow out of the WOA-Box with this estimation is 1.9 ± 0.2 Sv, which is in agreement with that estimated by Alves et al. (2011). The value we actually obtain is 1.2 Sv, lower than that indicated by other authors (2–3 Sv, Zenk, 1975; 1.9 Sv, Rhein and Hinrichsen, 1993; 2.3 Sv, Álvarez et al., 2005). These differences could come from the smoothed character of the climatological data. From four repeated cruises (July 1999, July 2000, November 2000, July 2001), Alves et al. (2011) estimated the entrainment of central waters at 1.2–1.7 Sv (a mean entrainment of 1.4 Sv, Figure 8), which is closer to the climatological values taking into account that they did not differentiate between entrainment *per se* and the central water recirculation. This value is also close to those values obtained in earlier studies from Baringer and Price (1997) (1.3 Sv) or S03 (1.6 ± 0.6 Sv). Even with the summer climatology (Figure 8, black values in brackets), when the OC appears intensified actual entrainment reaches only 1 Sv and the resulting MW outflow is 1.6 Sv. In contrast, Álvarez et al. (2005) represented an upper bound for the estimations, whose results are of the same order as Rhein and Hinrichsen (1993). Note, however, Rhein and Hinrichsen (1993) made their computations based on 1 Sv of MOW, which nowadays is known to be too high, inflating their estimates by 30%.

4. Summary and concluding remarks

657 By means of an inverse box model applied to World Ocean Atlas (WOA, 2009) data,
658 different components of the circulation in the Azores-Gibraltar Strait region were
659 estimated, with particular focus on the mean and seasonal circulation patterns and
660 overturning circulation system.

661 The upper general circulation pattern in the Azores-Madeira-Gibraltar Strait region
662 consisted of the well-identified anticyclonic circulation cell, taking part of the broader
663 basin-scale Subtropical Gyre with a permanent character throughout the year but
664 slightly enhanced in spring. Seasonal mean-climatic variability of the currents system
665 was derived. The principal currents identified from the WOA09 climatological data
666 were the Azores Current and Azores Counter Current across the western section, the
667 Portugal Current and the predominantly winter and autumn Iberian Poleward Current
668 across the northern section and finally, the Canary Current across the southern section.

669 The annual Azores Current transport, mostly confined to the upper 1000–1500
670 dbar, was quantified as 6.5 ± 0.8 Sv at 19.5°W , varying seasonally from its lowest value
671 in spring (5.3 ± 0.8 Sv), to its maximum in autumn (higher velocity maximum
672 accompanied by a deepening and broadening of the current). The absolute maximum of
673 the Azores Current occurs in January (10.2 ± 0.9 Sv). The Azores Counter Current
674 appeared intensified in spring and autumn ($> 3 \pm 0.9$ Sv) with lower transports in summer
675 and winter ($< 2 \pm 0.8$ Sv). Autumn is the season when the Azores Counter Current
676 becomes more easily identifiable as a westward jet. From the monthly variability of
677 both zonal currents, we suggested a seasonally varying ratio between them with the
678 Azores Current doubling the Counter Current in spring and autumn but with a higher-
679 than-two ratio of the Azores Current and Azores Counter Current in summer and winter.
680 Regarding the meridional Portugal and Canary Currents, their seasonal signal responded
681 to favourable spring-summer Subtropical Gyre intensification and favourable upwelling
682 conditions, exhibiting maximum transports of 5.20 ± 0.3 Sv (April) and -8.0 ± 0.4 Sv
683 (June), respectively. In addition, as part of the Portugal Current system and reducing the

684 net southward transport of the Portugal Current in autumn/winter, the Iberian Poleward
685 Current was quantified at 0.2 ± 0.1 Sv with a maximum northward transport in January
686 (1 ± 0.1 Sv); however, it was absent between the months of May to August.

687 The vertical structure of the circulation involved a relatively fresh upper layer of
688 central waters flowing into the area across the northern and western WOA sections, part
689 entraining the intermediate layer and part entering the Mediterranean Sea, together with
690 a high-salinity intermediate layer of Mediterranean Outflow Water flowing out of the
691 Strait of Gibraltar and ultimately, out of the WOA-Box along two principal advective
692 (northward and westward) paths. The overturning circulation induced by the central
693 water entrainment to the intermediate layer was quantified at 2.2 ± 0.1 Sv (annual mean),
694 for which the magnitude was enhanced in summer (2.6 ± 0.1 Sv) and reduced by 1 Sv
695 from autumn to spring (1.7 ± 0.2 Sv). From summer/autumn to spring, its depth
696 decreased progressively. The density level dividing the vertical circulation structure into
697 the upper-inflowing and lower-outflowing limbs of the overturning circulation (σ_{OC})
698 was identified at $\sigma_1 = 31.65 \text{ kg m}^{-3}$, which is above the isopycnal that typically separates
699 Central and Mediterranean Water ($\sigma_1 = 31.8 \text{ kg m}^{-3}$).

700

701 In terms of water masses, we focused on the spread of Mediterranean water at
702 intermediate levels and found that when the northward Mediterranean Water branch
703 weakens in spring and autumn, the westward Mediterranean Water vein strengthens and
704 vice versa. The maximum net transports across northern and western sections of the box
705 were -1.9 ± 0.6 Sv (summer) and -0.8 ± 0.2 Sv (spring), respectively. The westward
706 Mediterranean Water flow recirculates such that a more diluted form re-entered the box
707 within the Azores Current (0.3 Sv annual mean), while the northward Mediterranean
708 Water flow hardly recirculates within the Portugal Current (0.03 Sv annual mean).
709 Climatically speaking, no significant (within the error 0.2 Sv) Mediterranean volume
710 transport across the southern section was found.

The water mass composition of the principal currents was established quantitatively; the Azores Current transports mainly Central Waters (90%) with 50% comprising the subtropical variety and an increased proportion of recirculated Madeira Mode Water in summer (24%). About 40% of the Azores Counter Current corresponds to the subpolar variety of Central Waters. Other important contributors are the Mediterranean Water (25%) and the recirculated Labrador Sea Water (20%). Both the Portugal and the Canary Currents transport mainly Central Waters ($> 95\%$). During spring, the contribution of the subpolar variety to the Portugal Current exceeds that of the subtropical, whereas during the autumn-winter period, this proportion reverses. On the other hand, 60% of the Canary Current belongs to the subtropical variety, which recirculates from the Azores Current. The contribution of the Madeira Mode Water increases in autumn at the expense of the drop in the subtropical contribution.

The annual estimate for the Central Water transformation in the Gulf of Cadiz was given at 1.2 Sv. Of this, 0.6 corresponds to downwelled central water that recirculates without mixing with the underlying Mediterranean Water and the other 0.6 corresponds to central water entrainment.

To conclude, two extreme states of circulation (spring/summer vs. autumn/winter) can be described:

- On the one hand, during spring/summer, the position of the Azores High introduces a strong northerly component in the wind field over the WOA-Box region (Figure 1). The Portugal Current and Canary Current transports reach their maximum transports in spring (absolute maximum transports in April and June, respectively), due to the enhancement of the coastal branches of both currents. Near the Gibraltar Strait, the strongest MOW flux also occurs during this period (April). In addition, the deep circulation is also slightly enhanced. The Azores Counter Current presents a relative maximum, leading to higher exportation of MW by its westward branch, while the climatological signal of the northern branch almost disappears during this

738 season. The higher contribution of the Portugal Current to the central water net
739 upper transport into the box makes it less saline and helps compensate for the E-P
740 term, which is higher in late-summer early-autumn. In July, the general flow pattern
741 in the Gulf of Cadiz is enhanced (Machín et al., 2006b) and central water inflow
742 through the Strait of Gibraltar increases relative to the rest of the year (Soto-
743 Navarro et al., 2010). Furthermore, in this season, we estimated that the central
744 water net transport into the WOA-Box and the MW net outflow (northern MW
745 branch) reach their maximum transports, leading to an increased overturning
746 circulation (2.6 ± 0.1 Sv).

747 - On the other hand, in autumn, the surface circulation system appears diminished,
748 except for the AC that presents higher transport, importing saltier central water into
749 the box. Machín et al. (2006b) showed that higher zonal eastward transports reach
750 the south of the Gulf of Cadiz (1 Sv of net eastward transport). As neither
751 entrainment nor central water inflow compensates for this increased transport, the
752 Iberian Poleward Current is expected to compensate for it. Summing up, the
753 overturning system appears to be “relaxed” (1.7 ± 0.1 Sv).

754
755 Much effort was spent in producing time-averaged pictures, which provided a
756 more reliable quantitative picture of the circulation than seen before. In view of the
757 present results and conclusions, doubts over the inhomogeneity of the climatological
758 data base (Wunsch, 1996) are assuaged by the higher quality of WOA09 and the six-
759 fold increase in station data over previous versions (Levitus et al., 1998). In fact,
760 currents such as the Azores Counter Current that could not be identified well by the
761 WOA94 data (Pingree et al., 1999) can be now delimited. Nevertheless, one cannot
762 disregard the obvious limitation of time averaging. The smoothing of the thermohaline
763 properties maxima and the horizontal gradients reduces the geostrophic velocities by up
764 to one order of magnitude in comparison with quasi-synoptic measurements. This fact

765 may restrain but does not reject the particular use of WOA data to deal with water
766 masses such as Mediterranean water, in which the (punctual) mesoscale meddy activity
767 contributes notably to the horizontal salt fluxes. With this issue in mind, the present
768 study illustrates a good example of how this kind of reprocessed hydrographic data can
769 be combined with inverse methodologies (inverse box model plus multiparameter water
770 masses analysis) leading to consistent results, as has been validated particularly in
771 section 3.1.1 and through the entire manuscript; thus, providing useful interpretation of
772 the seasonal dynamics.

773 In further extension of this work, direct comparisons of the climatology results
774 with a quasi-synoptic cruise for a similar box in the same area will be developed, paying
775 attention to discrepancies in terms of horizontal salt fluxes and water masses
776 transformations.

778 **Acknowledgements**

779 This work is embraced within the CAIBEX Project: *Shelf-ocean exchanges in the*
780 *Canaries-Iberia Large Marine Ecosystem* (CTM2007-66408-C02/MAR), supported by
781 the Spanish Council of Education and Science. The first author is funded by a
782 predoctoral fellowship (FPU) of the Formation National Program of Human Resources,
783 within the framework of the National Plan of Scientific Investigation, Development and
784 Technologic Innovation 2008-2011, from the Spanish Council of Education. Thank you
785 very much to Professor E.D. Barton for his invaluable help with the English review. We
786 also thank the editor and the two anonymous reviewers for their helpful comments and
787 suggestions, which have greatly contributed to improve the original manuscript.

788 **References**

- 789 Álvarez, M., 2002. Water masses and transports of physical and chemical properties in
790 the Subpolar North Atlantic Gyre. Ph.D. Thesis, University of Vigo, Spain,
791 unpublished.
- 792 Álvarez, M., Álvarez-Salgado, X.A., 2009. Chemical tracer transport in the eastern
793 boundary current system of the North Atlantic. *Cienc Mar* 35, 123-139.
- 794 Álvarez, M., Pérez, F.F., Shoosmith, D.R., Bryden, H., 2005. Unaccounted role of
795 Mediterranean Water in the drawdown of anthropogenic carbon. *J Geophys Res*
796 110, C09S03. <http://dx.doi.org/10.1029/2004JC002633>.
- 797 Álvarez-Salgado, Figueiras, F.G., Perez, F.F., Groom, S., Nogueira, E., Borges, A.V.,
798 Chou, L., Castro, C.G., Moncoiffe, G., Ríos, A.F., Miller, A.E.J., Frankignoulle,
799 M., Savidge, G., Wollast, R., 2003. The Portugal coastal counter current off NW
800 Spain: new insights on its biogeochemical variability. *Prog Oceanogr* 56, 281-
801 321.
- 802 Alves, M., Carton, X., Ambar, I., 2011. Hydrological Structure, Circulation and Water
803 Mass Transport in the Gulf of Cadiz. *Int J Geosci* 2, 432-456.
- 804 Alves, M., Gaillard, F., Sparrow, M., Knoll, M., Giraud, S., 2002. Circulation patterns
805 and transport of the Azores Front-Current system. *Deep-Sea Res* 49 (19), 3983-
806 4002.
- 807 Ambar, I., Armi, L., Bower, A., Ferreira, T., 1999. Some aspects of time variability of
808 the Mediterranean Water off South Portugal. *Deep-Sea Res I* 46, 1109-1136.
- 809 Ambar, I., Howe, M.R., 1979a. Observations of the Mediterranean outflow-I: Mixing in
810 the Mediterranean outflow. *Deep-Sea Res I* 26A, 535-554.
- 811 Ambar, I., Howe, M., 1979b. Observations of the Mediterranean Outflow-II: The deep
812 circulation in the vicinity of the Gulf of Cadiz. *Deep-Sea Res I* 26A, 555-568.
- 813 Antonov, J.I., Seidov, D., Boyer, T.P., Locarnini, R.A., Mishonov, A.V., Garcia, H.E.,
814 Baranova, O.K., Zweng, M.M., Johnson, D.R., 2010. *World Ocean Atlas 2009*,

- 815 Volume 2: Salinity. Levitus, S. (Ed.), NOAA Atlas NESDIS 69, U.S. Gov.
816 Printing Office, Washington D.C., 184 pp.
- 817 Arhan, M.A., Colin de Verdière, A., Memery, L., 1994. The eastern boundary of the
818 subtropical North Atlantic. *J Phys Oceanogr* 24, 1295-1316.
- 819 Armi, L., Hebert, D., Oakey, N., Price, J.M., Richardson, P.L., Rossby, H.T., Ruddick,
820 B., 1989. Two Years in the Life of a Mediterranean Salt Lens. *J Phys Oceanogr*
821 19, 354-370.
- 822 Baringer, M., Price, J.F., 1997. Mixing and Spreading of the Mediterranean Outflow. *J*
823 *Phys Oceanogr* 27, 1654-1677.
- 824 Barton, E.D., 1998. Eastern boundary of the North Atlantic: Northwest Africa and
825 Iberia. In: Brink, K.H., Robinson, A.R. (Eds.), *The Sea*, Volume 11, Chapter 22,
826 *The Global Coastal Ocean: Regional Studies and Syntheses*, Harvard Univ. Press,
827 New York, pp. 633-657.
- 828 Barton, E.D., 2001. Ocean Currents: Atlantic Eastern Boundary - Canary Current/
829 Portugal Current. In: Steele, J., Thorpe, S., Turekian, K. (Eds.), *Encyclopaedia of*
830 *Ocean Sciences*, Volume 1, Academic Press, London, pp. 380-389.
- 831 Bower, A.S., Armi, L., Ambar, I., 1995. Direct evidence of meddy formation off the
832 southwestern coast of Portugal. *Deep-Sea Res. I*, 42, 1621-1630.
- 833 Bower, A.S., Armi, L., Ambar, I., 1997. Lagrangian observations of meddy formation
834 during a Mediterranean Undercurrent Seeding Experiment. *J Phys Oceanogr* 27,
835 2545-2575.
- 836 Boyer, T.P., Antonov, J.I., Baranova, O.K., Garcia, H.E., Johnson, D.R., Locarnini,
837 R.A., Mishonov, A.V., O'Brien, T.D., Seidov, D., Smolyar, I.V., Zweng, M.M.,
838 2009. *World Ocean Database 2009*, Chapter 1, Introduction, Levitus, S. (Ed.),
839 NOAA Atlas NESDIS 66, U.S. Gov. Printing Office, Washington D.C., 216 pp.
- 840 Carracedo, L.I., Pardo, P.C., Villaceros-Robineau, N., De la Granda, F., Gilcoto, M.,
841 Pérez F.F., 2012. Temporal changes of the water masses distribution and

- 842 transports along the 20°W CAIBOX section (NE Atlantic). *Cienc Mar* 38 (1B),
843 263-286.
- 844 Comas-Rodríguez, I., Hernández-Guerra, A., Fraile-Nuez, E., Martínez-Marrero, A.,
845 Benítez-Barrios, V.M., Pérez-Hernández, M.D., Vélez-Belchí, P., 2011. The
846 Azores Current System from a meridional section at 24.5°W. *J Geophys Res* 116,
847 C09021. <http://dx.doi.org/10.1029/2011JC007129>.
- 848 Criado-Aldeanueva, F., García-Lafuente, J., Vargas, J.M., Del Río, J., Vázquez, A.,
849 Reul, A., Sánchez, A., 2006. Distribution and circulation of water masses in the
850 Gulf of Cadiz from in situ observations. *Deep-Sea Res II* 53, 1144-1160.
- 851 Dickson, R.R., Gould, W.J., Muller, T.J., Maillard, C., 1985. Estimates of the Mean
852 Circulation in the Deep (>2000m) Layer of the Eastern North Atlantic. *Prog*
853 *Oceanogr* 14, 103-127.
- 854 Fajar, N.M., Pardo, P.C., Carracedo, L.I., Vázquez-Rodríguez, M., Ríos, A.F., Pérez, F.,
855 2012. Trends of the anthropogenic CO₂ along 20°W in the Iberian Basin. *Cienc*
856 *Mar* 38 (1B), 287-306.
- 857 Fraile-Nuez, E., Machín, F., Vélez-Belchí, P., López-Laatzén, F., Borges, R.,
858 Benítez-Barrios, V., Hernández-Guerra, A., 2010. Nine years of mass transport
859 data in the eastern boundary of the North Atlantic Subtropical Gyre. *J Geophys*
860 *Res* 115, C09009. <http://dx.doi.org/10.1029/2010JC006161>.
- 861 Frouin, R., Fiúza, A. F. G., Ambar, I., Boyd, T. J., 1990. Observations of a poleward
862 surface current off the coasts of Portugal and Spain during winter. *J Geophys Res*
863 95, 679-691.
- 864 Fusco, G., Artale, V., Cotroneo, Y., Sannino, G., 2008. Thermohaline variability of
865 Mediterranean Water in the Gulf of Cadiz: 1948-1999. *Deep-Sea Res I* 55, 1624-
866 1638.
- 867 Ganachaud, A., Wunsch, C., 2000. Improved estimates of global ocean circulation, heat
868 transport and mixing from hydrographic data. *Nature* 408, 453-457.

- 869 Ganachaud, A., Wunsch, C., Marotzke, J., Toole, J., 2000. Meridional overturning and
870 large-scale circulation of the Indian Ocean. *J Geophys Res* 105, 26117-26134.
- 871 García-Lafuente, J., Sánchez-Román, A., Díaz del Río G., Sannino, G., Sánchez-
872 Garrido, J. C., 2007. Recent observations of seasonal variability of the
873 Mediterranean outflow in the Strait of Gibraltar, *J Geophys Res.* 112, C10005,
874 doi:10.1029/2006JC003992.
- 875 Haynes, R., Barton, E.D., 1990. A poleward flow along the Atlantic coast of the Iberian
876 Peninsula. *J Geophys Res* 95, 11425-11441.
- 877 Hernandez-Guerra, A., Fraile-Nuez, E., Lopez-Laatzén, R.F., Martínez, A., Parrilla G.,
878 Vélez-Belchí, P., 2005: Canary Current and North Equatorial Current form an
879 inverse box model. *J Geophys Res* 110, C12019.
880 <http://dx.doi.org/10.1029/2005JC003032>.
- 881 Huertas, I. E., Ríos, A. F., García-Lafuente, J., Navarro, G., Makaoui, A., Sánchez-
882 Román, A., Rodríguez-Galvez, S., Orbi, A., Ruíz, J., Pérez, F. F., 2012. Atlantic
883 forcing of the Mediterranean oligotrophy. *Global Biogeochem Cycles* 26, GB2022.
884 <http://dx.doi.org/10.1029/2011GB004167>.
- 885 Jia, Y., 2000. Formation of an Azores Current due to Mediterranean Overflow in a
886 Modelling Study of the North Atlantic. *J Phys Oceanogr* 30, 2342-2358.
- 887 Karstensen, J., Tomczak, M., 1998. Age determination of mixed water masses using
888 CFC and oxygen data. *J Geophys Res* 103, 18599-18610.
- 889 Kida, S., Price, J.F., Yang, J., 2008. The Upper-Oceanic Response to Overflows: A
890 Mechanism for the Azores Current. *J Phys Oceanogr* 38, 880-895.
- 891 Klein, B., Siedler, G., 1989. On the Origin of the Azores Current. *J Geophys Res* 94,
892 6159-6168.
- 893 Levitus, S., Boyer, T.P., Conkright, M.E., O' Brien, T., Antonov, J., Stephens, C.,
894 Stathoplos, L., Johnson, D., Gelfeld, R., 1998. World Ocean Database 1998,

- 895 Volume 1: Introduction. Levitus, S. (Ed.), NOAA Atlas NESDIS 18, U.S. Gov.
896 Printing Office, Washington D.C., 346pp.
- 897 Lherminier, P., Mercier, H., Gourcuff, C., Alvarez, M.F., Bacon, S., Kermabon, C.,
898 2007. Transport across the 2002 Greenland-Portugal section and comparison with
899 1997. *J Geophys Res* 112, C07003. <http://dx.doi.org/10.1029/2006JC003716>.
- 900 Lherminier, P., Mercier, H., Huck, T., Gourcuff, C., Pérez, F.F., Morin, P., Sarafanov,
901 A., Falina, A., 2010. The Atlantic Meridional Overturning Circulation and the
902 subpolar gyre at the A25-OVIDE section in June 2002 and 2004. *Deep-Sea Res I*
903 57 (11), 1374-1391.
- 904 Locarnini, R.A., Mishonov, A.V., Antonov, J.I., Boyer, T.P., Garcia, H.E., Baranova,
905 O.K., Zweng, M.M., Johnson, D.R., 2010. *World Ocean Atlas 2009, Volume 1:*
906 *Temperature*. Levitus, S. (Ed.), NOAA Atlas NESDIS 68, U.S. Gov. Printing
907 Office, Washington D.C., 184 pp.
- 908 Louarn, E., and Morin, P., 2011. Antarctic Intermediate Water influence on
909 Mediterranean Sea Water outflow, *Deep-Sea Res I*, 58(9), 932-942,
910 doi:10.1016/j.dsr.2011.05.009.
- 911 Lux, M., Mercier, H., Arhan, M., 2001. Inter hemispheric exchanges of mass and heat
912 in the Atlantic Ocean in January-March 1993. *Deep-Sea Res I* 48 (3), 605-638.
- 913 Machín, F., Hernández-Guerra, A., Pelegrí, J.L., 2006a. Mass fluxes in the Canary
914 Basin. *J Progr Oceanogr* 70, 416-447.
- 915 Machín, F., Pelegrí, J.L., 2009. Northward Penetration of Antarctic Intermediate Water
916 off Northwest Africa. *J Phys Oceanogr* 39, 512-535.
- 917 Machín, F., Pelegrí, J.L., Marrero-Díaz, A., Laiz, I., Ratsimandresy, A.W., 2006b. Near-
918 surface circulation in the southern Gulf of Cadiz. *Deep-Sea Res II* 53, 1161-1181.
- 919 Mazé, J.P., Arhan, M., Mercier H., 1997. Volume budget of the eastern boundary layer
920 off the Iberian Peninsula. *Deep-Sea Res I* 44, 1543-1574.

- 921 McCartney, M.S. 1992. Recirculating components to the deep boundary current of the
922 northern North Atlantic. *Prog Oceanogr* 29, 283-383.
- 923 McCartney, M.S., Bennet, S.L., Woodgate-Jones, M.E., 1991. Eastward Flow through
924 the Mid-Atlantic Ridge at 11°N and its Influence on the Abyss of the Eastern
925 Basin. *J Phys Oceanogr* 21, 1081-1121.
- 926 Mercier, H., 1986. Determining the General Circulation of the Ocean: A Non Linear
927 Inverse Problem. *J Geophys Res* 91 (C4), 5103-5109.
- 928 Navarro-Pérez, E., Barton E.D., 2001. Seasonal and interannual variability of the
929 Canary Current. *Sci Mar* 65, 205-213.
- 930 New, A.L., Jia, Y., Coulibaly, M., Dengg, J., 2001. On the role of the Azores Current in
931 the ventilation of the North Atlantic Ocean. *Progr Oceanogr* 48, 163-194.
- 932 Onken, R., 1992. The Azores Countercurrent. *J Geophys Oceanogr* 23, 1638-1646.
- 933 Paillet, J., Mercier, H., 1997. An inverse model of the eastern North Atlantic general
934 circulation and thermocline ventilation. *Deep-Sea Res* 44 (8), 1293-1328.
- 935 Pardo, P.C., Pérez, F.F., Velo, A., Gilcoto, M., 2012. Water masses distribution in the
936 Southern Ocean: Improvement of an extended OMP (eOMP) analysis. *Progr*
937 *Oceanogr* 103, 92-105.
- 938 Péliz, A., Dubert, J., Haidvogel, D.B., LeCann, B., 2003. Generation and unstable
939 evolution of a density-driven Eastern Poleward Current: The Iberian Poleward
940 Current. *J Geophys Res* 108 (C8), 3268. <http://dx.doi.org/0.1029/2002JC001443>.
- 941 Péliz, A., Dubert, J., Santos, A.M.P., Oliveira, P.B., LeCann, B., 2005. Winter upper
942 ocean circulation in the western Iberian basin, fronts, eddies and poleward flows:
943 an overview. *Deep-Sea Res I* 52 (4), 621-646.
- 944 Péliz, A., Marchesiello, P., Santos, A.M.P., Dubert, J., Teles-Machado, A., Marta-
945 Almeida, M., Le Cann, B., 2009. Surface circulation in the Gulf of Cadiz: 2.
946 Inflow-outflow coupling and the Gulf of Cadiz slope current. *J Geophys Res* 114,
947 C03011. <http://dx.doi.org/10.1029/2008JC004771>.

- 948 Pérez, F.F., Gilcoto, M., Ríos, A.F., 2003. Large and mesoscale variability of the water
949 masses and the deep chlorophyll maximum in the Azores Front. *J Geophys Res*
950 108 (C7), 3215-3233.
- 951 Pérez, F.F., Mintrop, L., Llina, O., González-Dávila, M., Castro, C., Álvarez, M.,
952 Körtzinger, A., Santana-Casiano, M., Rueda, M.J., Ríos, A.F., 2001. Mixing
953 analysis of nutrients, oxygen and inorganic carbon in the Canary Islands Region. *J*
954 *Marine Syst* 28 (3-4), 183-201.
- 955 Pingree, R.D., Garcia-Soto, C., Sinha, B., 1999. Position and structure of the
956 Subtropical/Azores Front region from combined Lagrangian and remote sensing
957 (IR/altimeter/SeaWiFS) measurements. *J Mar Biol* 79, 769-792.
- 958 Polzin, K.L., Toole, J.M., Ledwell, J.R., Schmitt, R.W., 1997. Spatial variability of
959 turbulent mixing in the Abyssal Ocean. *Nature* 276, 93-96.
- 960 Reid, J.L., 1994. On the total geostrophic circulation of the North Atlantic Ocean: Flow
961 patterns, tracers, and transports. *Progr Oceanogr* 33, 1-92.
- 962 Rhein, M., Hinrichsen, H.H., 1993. Modification of Mediterranean Water in the Gulf of
963 Cadiz, studied with hydrographic, nutrient and chlorofluoromethane data. *Deep-*
964 *Sea Res I* 40 (2), 267-291.
- 965 Richardson, P.L., Bower, A.S., Zenk, Walter, 2000. A census of Meddies tracked by
966 floats. *Progr Oceanogr* 45, 209-250.
- 967 Ríos, A.F., Pérez, F.F., Fraga F., 1992. Water masses in the upper and middle North
968 Atlantic Ocean east of the Azores. *Deep-Sea Res II* 39 (3/4), 645-658.
- 969 Saunders, P.M., 1982. Circulation in the eastern North Atlantic. *J Mar Res* 40, 641-657.
- 970 Shapiro, G.I., Meschanov, S.L., 1996. Spreading pattern and mesoscale structure of
971 Mediterranean outflow in the Iberian Basin estimated from historical data. *J*
972 *Marine Syst* 7, 337-348.
- 973 Siedler, G., Kuhl, A., Zenk, W., 1987. The Madeira mode water. *J Phys Oceanogr* 17,
974 1561-1970.
-

- 975 Slater, D.R., 2003. The Transport of Mediterranean Water in the North Atlantic Ocean.
976 Ph.D. Thesis, University of Southampton, UK, unpublished.
- 977 Smith, R.D., Maltrud, M.E., 1999. Numerical Simulation of the North Atlantic Ocean at
978 $1/10^\circ$. J Phys Oceanogr 30, 1532-1561.
- 979 Soto-Navarro, J., Criado-Aldeanueva, F., García-Lafuente, J., Sánchez-Román, A.,
980 2010. Estimation of the Atlantic inflow through the Strait of Gibraltar from
981 climatological and in situ data. J Geophys Res 115, C10023.
982 <http://dx.doi.org/10.1029/2010JC006302>
- 983 Stramma, L., Siedler, F., G., 1988. Seasonal changes in the North Atlantic Subtropical
984 Gyre. J Geophys Res 93, 8111-8118.
- 985 Tsuchiya, M., Talley, L.D., McCartney, M.S., 1992. An eastern Atlantic section from
986 Iceland southward across the equator. Deep-Sea Res I 39, 1885-1917.
- 987 van Aken, H.M., 2000a. The hydrography of the mid-latitude northeast Atlantic Ocean.
988 I: The deep water masses. Deep-Sea Res I 47 (5), 757-788.
- 989 van Aken, H.M., 2000b. The hydrography of the mid-latitude northeast Atlantic Ocean
990 II: The intermediate water masses. Deep-Sea Res I 47 (5), 789-824.
- 991 Wunsch, C., 1977. Determining the general circulation of the oceans: A preliminary
992 discussion. Science 196, 871-875.
- 993 Wunsch, C., 1978. The North Atlantic general circulation West of 50°W determined by
994 inverse methods. Rev Geophys Space Phys 16, 583-620.
- 995 Wunsch, C., 1996. The ocean circulation inverse problem. Cambridge University Press,
996 Cambridge.
- 997 Zenk, W., 1975. On the Mediterranean outflow west of Gibraltar. Meteor Forsch.-
998 Ergebn., 16, 23-24
999

1000

1001 Table 1. a) Summary of the annual constraints, b) seasonal change in volume and salt
1002 constraints (T_I).

1003

CONSTRAINT	TEST	VALUE	HORIZONTAL DOMAIN VERTICAL DOMAIN	AFTER INVERSION
Surface-to-bottom volume conservation (Sv)	T_0, T_I	$0 \pm 0.1, 0.071 \pm 1$	Entire box Entire water column	$-0.04 \pm 0.1, 0.01 \pm 1$
Surface-to-bottom salt conservation ($\times 10^9$ kg/s)	T_0, T_I	$-1.55 \pm 0.2, 0 \pm 10^{-3}$	Entire box Entire water column	$-1.55 \pm 0.2, 0 \pm 10^{-3}$
Volume, salt and heat conservation by deep layers	T_0, T_I	$0 \pm K, A \delta \Phi / \delta z$	Entire box $\sigma_2 > 41.430 \text{ kg/m}^3$ (~2600 m to bottom)	$-0.01-0, 0.02-0.08$
Surface-to-bottom LSW+ISOW+NEADWL conservation (Sv)	T_I	0 ± 0.2	Entire box See WM distribution, Figure 5a	-0.39 ± 0.2
(1) NEADWL-IAP transport (Sv)	T_I	-0.8 ± 0.8	North section (St pairs 1-10) $\sigma_2 > 45.85 \text{ kg/m}^3$ (~3700 m to bottom)	-0.56 ± 0.8
(2) SADC-based transport (Lherminier et al., 2010) (Sv)	T_I	-1 ± 2	Eastern Boundary Current (St pairs 1-2) $\sigma_2 > 36.94 \text{ kg/m}^3$ (~2000 m to bottom)	-0.08 ± 2
(3) Central water off Africa coast transport (Fraile-Nuez et al., 2010) (Sv)	T_I	-0.81 ± 0.5	Lanzarote Passage (St pairs 29-30) Surface to $\gamma = 27.3 \text{ kg/m}^3$ (0-600 m)	-1.83 ± 0.5
(4) AA off Africa coast transport (Fraile-Nuez et al., 2010) (Sv)	T_I	0.09 ± 0.5	Lanzarote Passage (St pair 30) $\gamma = 27.3 \text{ kg/m}^3$ to $\gamma = 27.7 \text{ kg/m}^3$ (600 ~1100 m)	0.21 ± 0.5

1004

	VOLUME (Sv)				SALT ($\times 10^9 \text{ kg/m}^3$)	
	AIR-SEA FLUX WOA-Box (E-P-R) (ERA40)	AIR-SEA FLUX MedSea (E-P-R) (ERA40)	VOLUME FLUX CONSTRAINT		SALT FLUX CONSTRAINT	
Winter (1-3)	-0.024	-0.026	0.050	± 1	0	± 0.001
Spring (4-6)	-0.032	-0.019	0.051	± 1	0	± 0.001
Summer (7-9)	-0.040	-0.051	0.091	± 1	0	± 0.001
Autumn (10-12)	-0.042	-0.051	0.093	± 1	0	± 0.001
Annual mean	-0.034	-0.034	0.071	± 1	0	± 0.001

1005

1006

1007

1008 Table 2. Correlation between the different overturning system components (linear
1009 regressions shown for T_l). R^2 is the determination coefficient at the 95% confidence
1010 interval (T_l (T_0)). The symbol * means that the component is ahead one month with
1011 respect to the other.

1012

	<i>LeastSquareFitting</i>	<i>R²</i>
<i>Portugal Current vs. Canary Current*</i>	$y = 0.84x + 3.97$	0.66 (0.60)
<i>Overturning Circulation vs. Central Water</i>	$y = 0.97x + 0.70$	0.94 (0.97)
<i>Overturning Circulation vs. Mediterranean Water</i>	$y = 0.66x - 0.30$	0.88 (0.70)
<i>Mediterranean Water vs. Central Water</i>	$y = 0.71x + 0.62$	0.90 (0.69)

1013

1014

1015

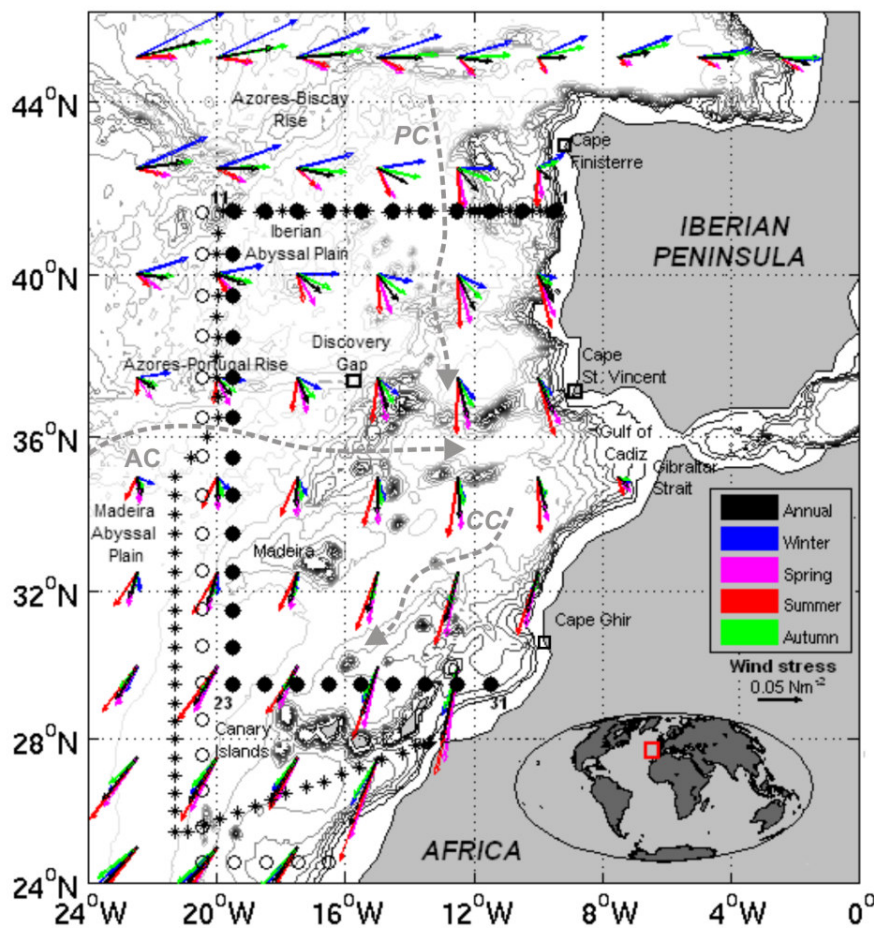
1016 List of the acronyms used in the text.

1017

<i>Currents</i>	
AC	Azores Current
ACC	Azores Counter Current
CC	Canary Current
PC	Portugal Current
<i>Water masses</i>	
AA	Antarctic Intermediate Water (diluted core)
ENACW _p	Subpolar East North Atlantic Central Water
ENACW _T	Subtropical East North Atlantic Central Water
H	Harvey
ISOW	Iceland Scotland Overflow Water
LSW	Labrador Sea Water
MMW	Madeira Mode Water
MOW	Mediterranean Outflow Water
MW	Mediterranean Water
MW _{nb}	Northward Mediterranean Water branch
MW _{wb}	Westward Mediterranean Water branch
NEADW _L	Lower North East Atlantic Deep Water
<i>Other abbreviations</i>	
OC	Overturning Circulation
WOA09	World Ocean Atlas 2009

1018 Figures

1019 Figure 1. WOA09 grid defining the box (black dots, labelled as nodes 1 to 31). The
 1020 MedBox (Álvarez et al., 2005) and Levitus-MedBox (Slater 2003) stations appear
 1021 superimposed (black stars and white dots, respectively). The seasonally-averaged wind
 1022 field is shown (see colour arrows legend). The figure also includes topographic features
 1023 cited throughout the text: Azores-Biscay Rise, Azores-Portugal Rise, Discovery Gap,
 1024 Iberian Abyssal Plain, Madeira Abyssal Plain, Gulf of Cadiz and Gibraltar Strait. Grey
 1025 dashed lines indicate main surface currents (PC, Portugal Current; AC, Azores Current;
 1026 CC, Canary Current).



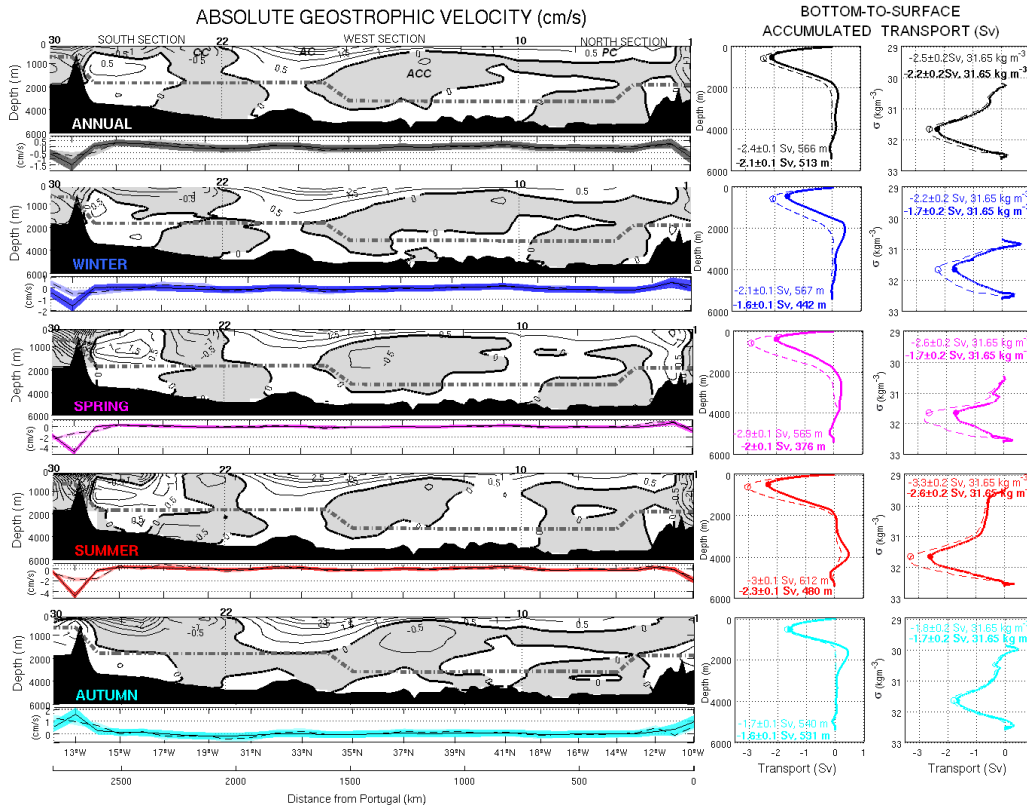
1027

1028

1029

1030 Figure 2. Left) Contour plots of absolute geostrophic currents for the WOA-Box (T_I)
 1031 (inside box view is set up). Grey shaded area indicates (negative) outgoing velocities
 1032 and white shaded area (positive) incoming velocities. Initial reference level is also
 1033 plotted (dashed-point grey line). Under-contour charts present reference level velocities
 1034 after inversion (black straight/dashed lines for T_I/T_0 , respectively) with their error
 1035 interval (shadings). Right) Charts of accumulated transports (Sv) in depth (left) and
 1036 density levels (right). Again, straight and dashed lines mean T_I and T_0 , respectively.

1037

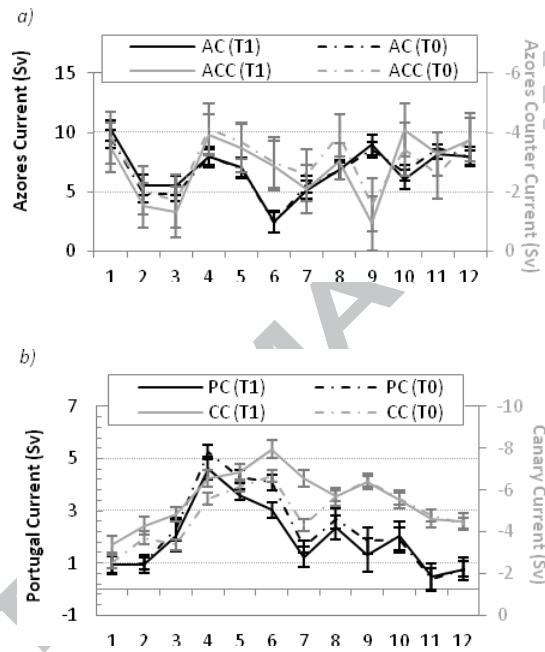


1038

1039

1040 Figure 3. Climatological monthly time series (January to December) of the main
 1041 currents of the WOA-Box surface-subsurface circulation, *a*) Azores Current (AC) and
 1042 Azores Counter Current (ACC) and *b*) Portugal Current (PC) and Canary Current (CC),
 1043 under different constraints (T_0 and T_I , see text).

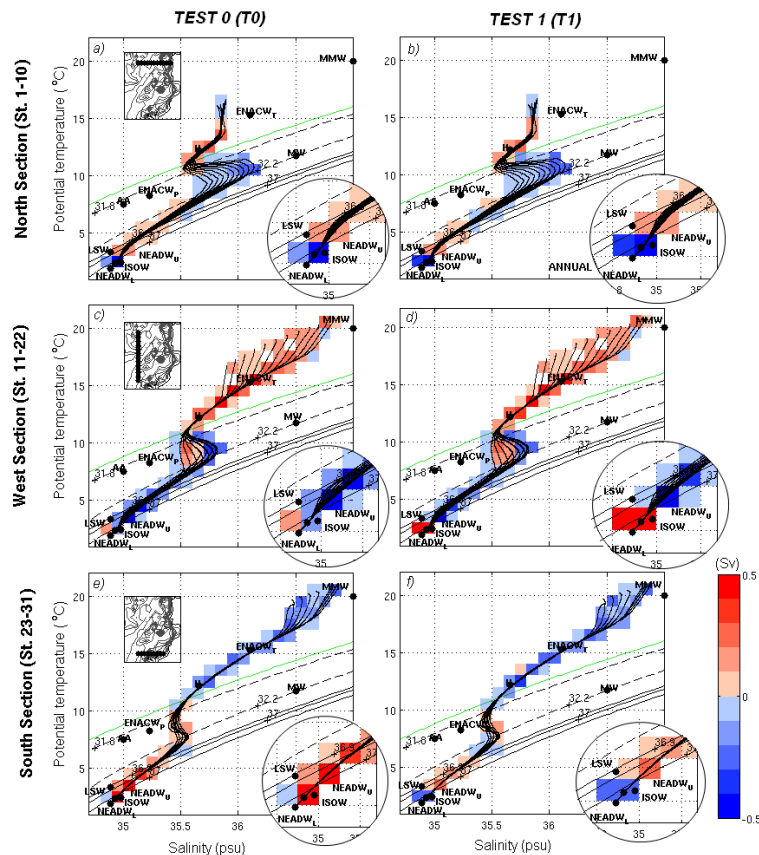
1044



1045

1046

1047 Figure 4. Potential temperature (surface reference level) vs. salinity diagrams for annual
1048 mean (T_0 left column, T_1 right column) and for Northern, Western and Southern sections
1049 (in rows from top to bottom). Dashed isolines correspond to potential density anomaly
1050 at 1000-m reference level ($\sigma_1 = 31.8$ and 32.25) and black thin isolines correspond to
1051 potential density anomaly at 2000-m reference level ($\sigma_2 = 36.89$, 36.95 and 37.05), all in
1052 kg m^{-3} . These isopycnals delimit the water masses into six regions: ENACW layer
1053 (surface to $\sigma_1 = 31.8$), MW layer ($\sigma_1 = 31.8$ to $\sigma_1 = 32.25$), MW-LSW layer ($\sigma_1 = 32.25$
1054 to $\sigma_2 = 36.89$), LSW layer ($\sigma_2 = 36.89$ to $\sigma_2 = 36.95$), deep mixed layer ($\sigma_2 = 36.95$ to σ_2
1055 $= 37.05$) and NEADW layer ($\sigma_2 = 37.05$ to bottom). Additionally, the isopycnal where
1056 the OC has been defined is also included ($\sigma_{OC} = 31.65 \text{ kg m}^{-3}$, green line). Black dots
1057 mark the position of the source water masses. Filled colour contours of transports (Sv)
1058 are given by bins of 0.5°C and 0.1 psu , positive (red) entering the WOA-Box.

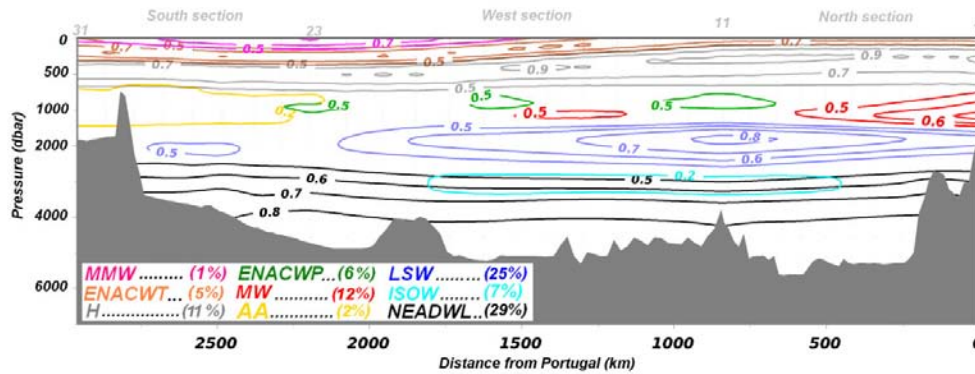


1059

1060

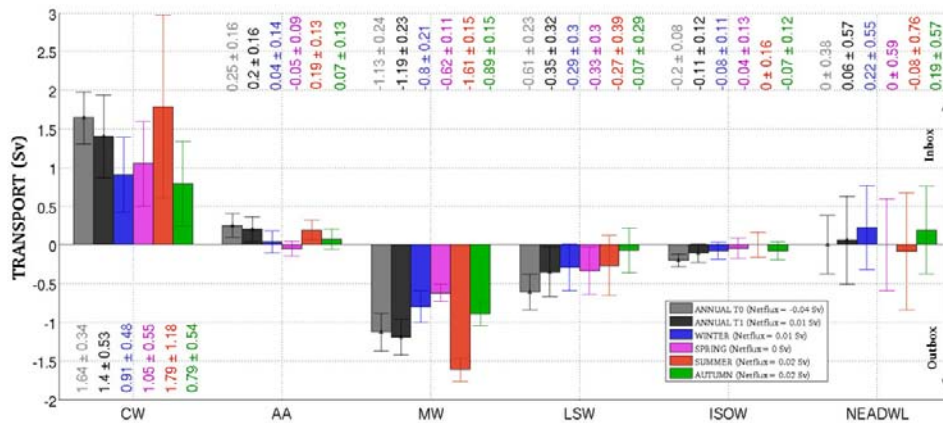
1061 Figure 5. eOMP results: a) water masses spatial distribution for annual mean. Contour
 1062 lines are plotted for contributions > 50%, except for the AA and ISOW, whose contour
 1063 lines represent a contribution > 20%. Note that vertical scale has been amplified in the
 1064 first 1000 dbar for clarity. Figures in parentheses in the legend are percentages of
 1065 occupied area by water mass (100% represents the area for the entire section). b) Bar
 1066 diagram for annual, seasonal and monthly water mass net transport in the WOA-Box.
 1067 Error bars are also shown for each period (errors given by inverse model).

1068 a)



1069

1070 b)



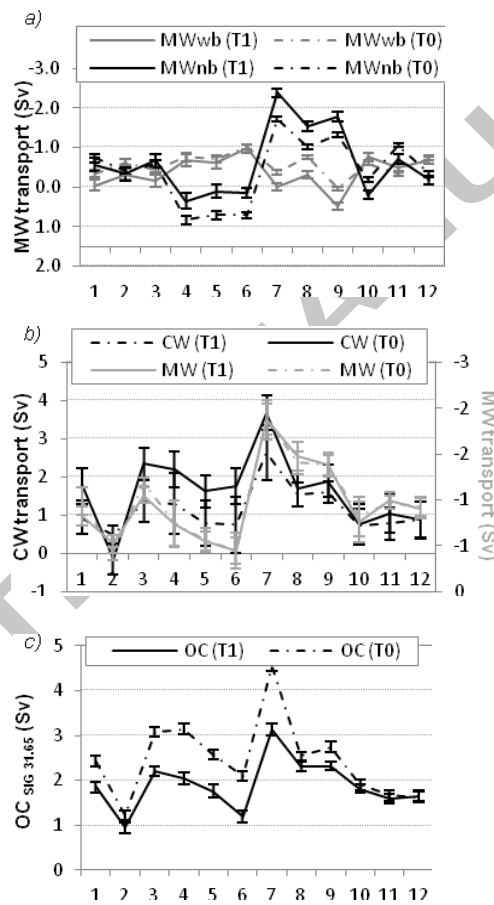
1071

1072

1073

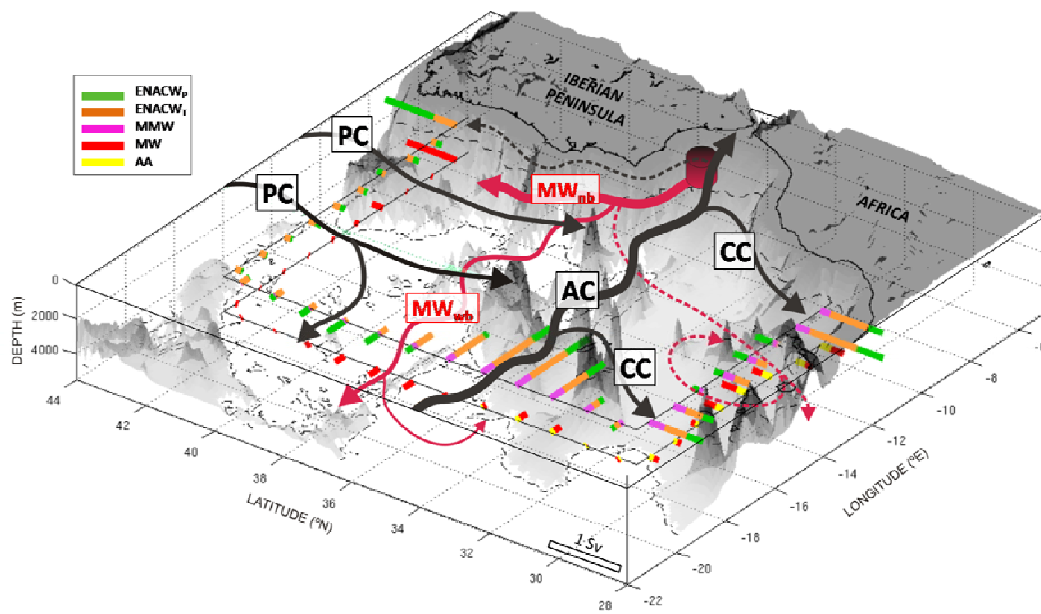
1074 Figure 6. Climatological monthly time series (January to December) of the main
1075 components of the OC system: *a)* Westward and Northward branches of the
1076 Mediterranean Water (MW_{wb} and MW_{nb} , respectively), *b)* MW and central waters net
1077 transports(whole box) and *c)* Overturning transport (OC).

1078



1079

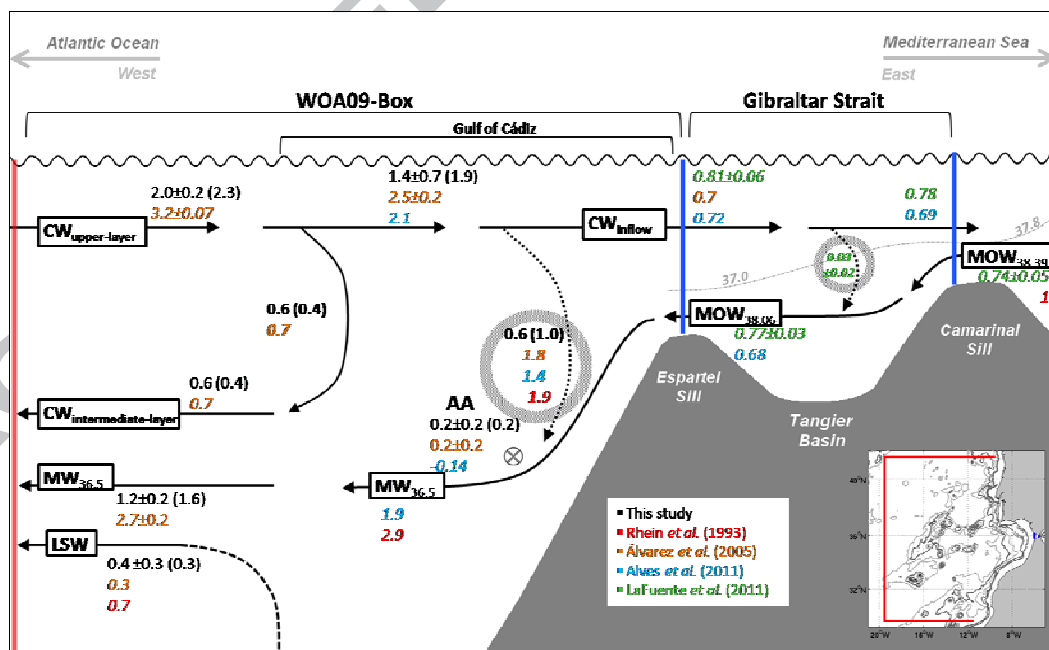
Figure 7. Schematic diagram of the circulation of the upper-intermediate (annual mean) circulation. The principal flows at these two horizontal levels are shown with black-red arrows, respectively. Black-to-red cylinder in the Gulf of Cadiz region represents the entrainment of central waters to the Mediterranean level. Stacked coloured bars represent horizontal transports (in Sv) between node stations. In the upper level, colour bars refer to the central waters: Subpolar East North Atlantic Central Water (green), Subtropical East North Atlantic Central Water (orange) and Madeira Mode Water (pink). In the lower level, colour bars refer to Mediterranean Water (red) and Antarctic Intermediate Water (yellow).



1091

1092 Figure 8. Schematic summary of mean exchanges (S_v), zoomed in on the Gulf of Cadiz
 1093 – Strait of Gibraltar region. Two boxes are delimited (from west to east): WOA09-Box
 1094 and Gibraltar Strait box. Dotted lines and grey circles indicate areas where Central
 1095 Water (CW) entrains and mixes with Mediterranean Outflow Water (MOW). Note, CW
 1096 comprises the sum of the Madeira Mode Water and subtropical and subpolar types of
 1097 East North Atlantic Central Water. Dashed line means Labrador Sea Water (LSW)
 1098 contribution to Mediterranean Water (MW) mixing. The small crossed open circle
 1099 marks the horizontal mix with the remnant Antarctic Intermediate Water (AA). Dashed-
 1100 dotted thin grey line denotes the interface of zero velocity between CW-Inflow/MOW
 1101 (grey numbers are the salinity values of the interface on the western and eastern sides of
 1102 the strait (Huertas et al., 2012)). WOA09-Annual Climatology results are given in black
 1103 numbers (WOA09-Summer values are given in parentheses) and results from the
 1104 literature are in colour. Vertical axis (in metres) is illustrative (not to scale).

1105



1106

1107